Characterization of Very Low Intensity Ion Beams from CERN REX/HIE-ISOLDE Linear Accelerator

Niels Bidault – Thesis Defence

BE-OP-ISO, CERN, 1211 Geneva 23, Switzerland
University of Rome 'La Sapienza' & INFN, 00185 Rome, Italy

Beam Quality

Beam Intensity Optimization

Slow extraction

Charge-breeding performances

Beam Purity

EBIS partial pressures

Rare contaminants

Transverse Beam Properties

Quadrupole-scan

Trace space reconstruction

Longitudinal Beam Properties

Beam energy distribution

Bunch structure

The CERN Accelerator Complex

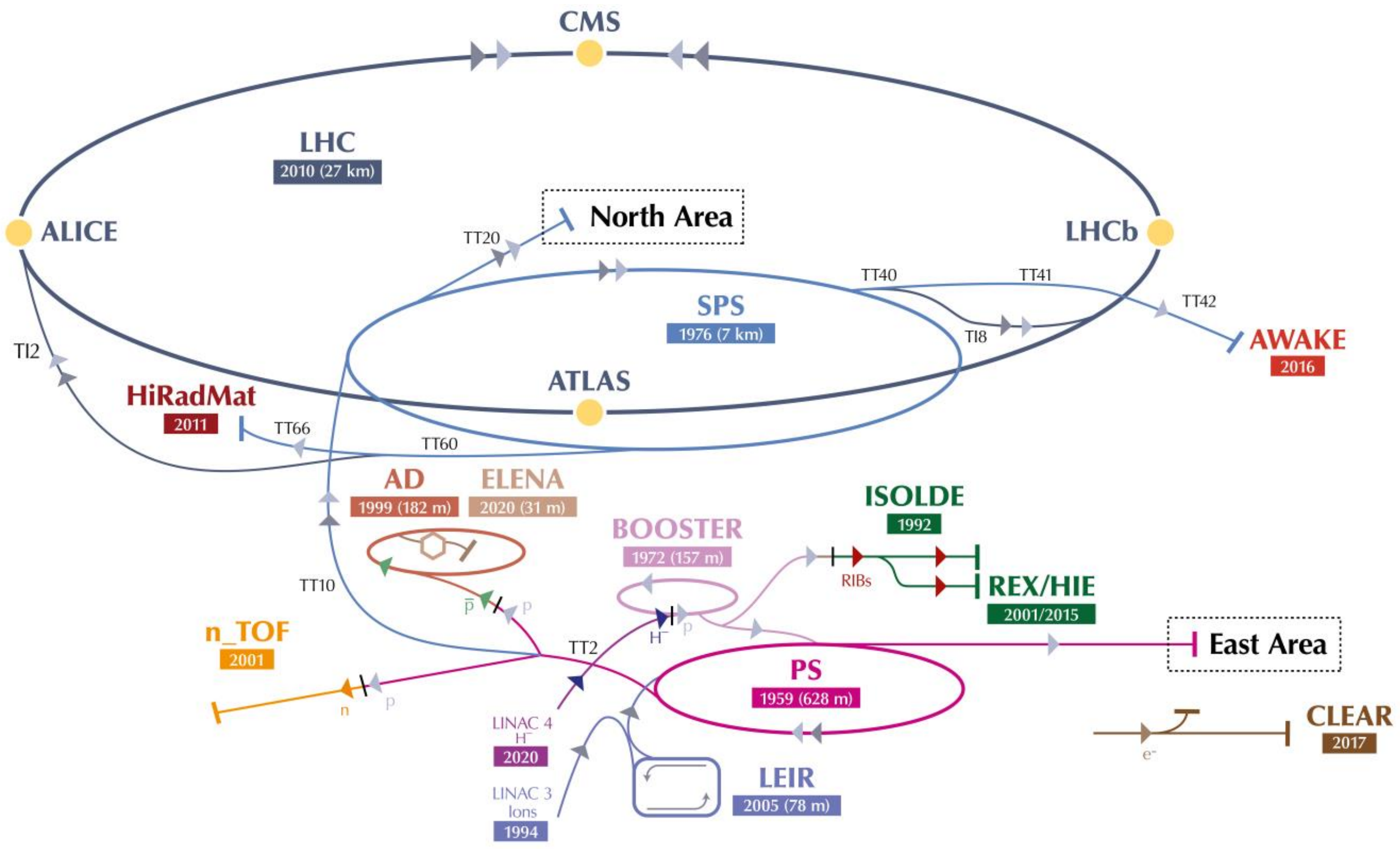

H⁻ (hydrogen anions) p (protons) ions RIBs (Radioactive Ion Beams) n (neutrons) p̄ (antiprotons) e⁻ (electrons)

LHC - Large Hadron Collider // SPS - Super Proton Synchrotron // PS - Proton Synchrotron // AD - Antiproton Decelerator // CLEAR - CERN Linear Electron Accelerator for Research // AWAKE - Advanced WAKefield Experiment // ISOLDE - Isotope Separator OnLine // REX/HIE - Radioactive EXperiment/High Intensity and Energy ISOLDE // LEIR - Low Energy Ion Ring // LINAC - LINear ACcelerator // n_TOF - Neutrons Time Of Flight // HiRadMat - High-Radiation to Materials

Research at ISOLDE

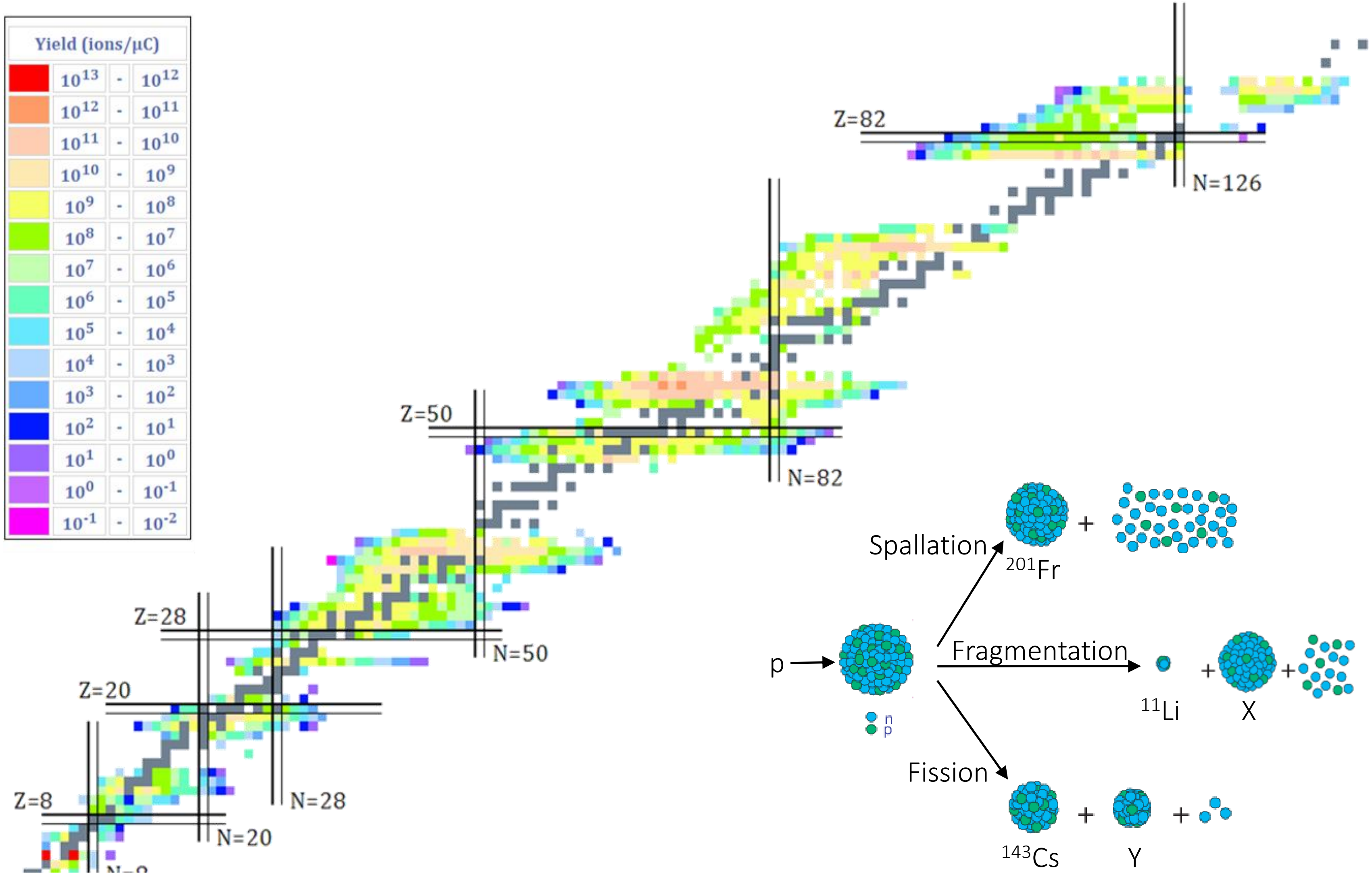

Research fields:

- Accelerator physics
- Astrophysics
- Biophysics
- B. S. M. physics
- Material science
- Medical applications
- Nuclear and Atomic physics

Figures of merit:

- 1200 isotopes
- 73 elements
- ~ 50 % of the CERN protons
- ~ 50 staff/students/fellow
- ~ 1500 users
- ~ 2000 hours/year of beamtime

Experimental Hall

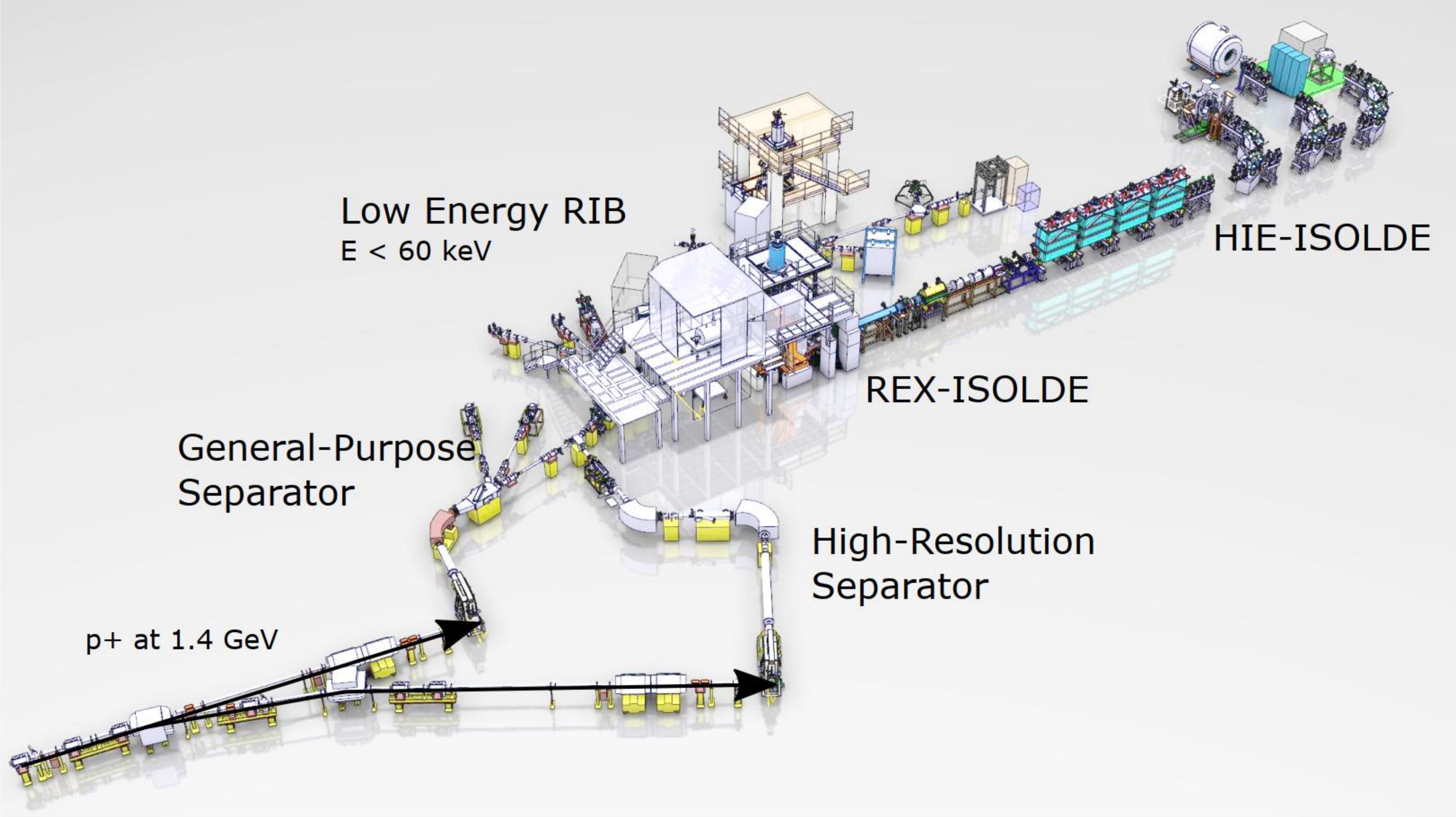

Beam Quality

Beam Intensity Optimization

Slow extraction

Charge-breeding performances

Beam Purity

EBIS partial pressures

Rare contaminants

Transverse properties

Quadrupole-scan

Trace space reconstruction

Longitudinal properties

Beam energy distribution

Bunch structure

REX-ISOLDE

- LaB6 cathode : I_{e-} < 250 mA (j < 100 A/cm2) $|U_{gun}|$< 5 kV
- IrCe cathode: I_{e-} < 300 mA (j < 400 A/cm2) $|U_{gun}|$< 6.5 kV

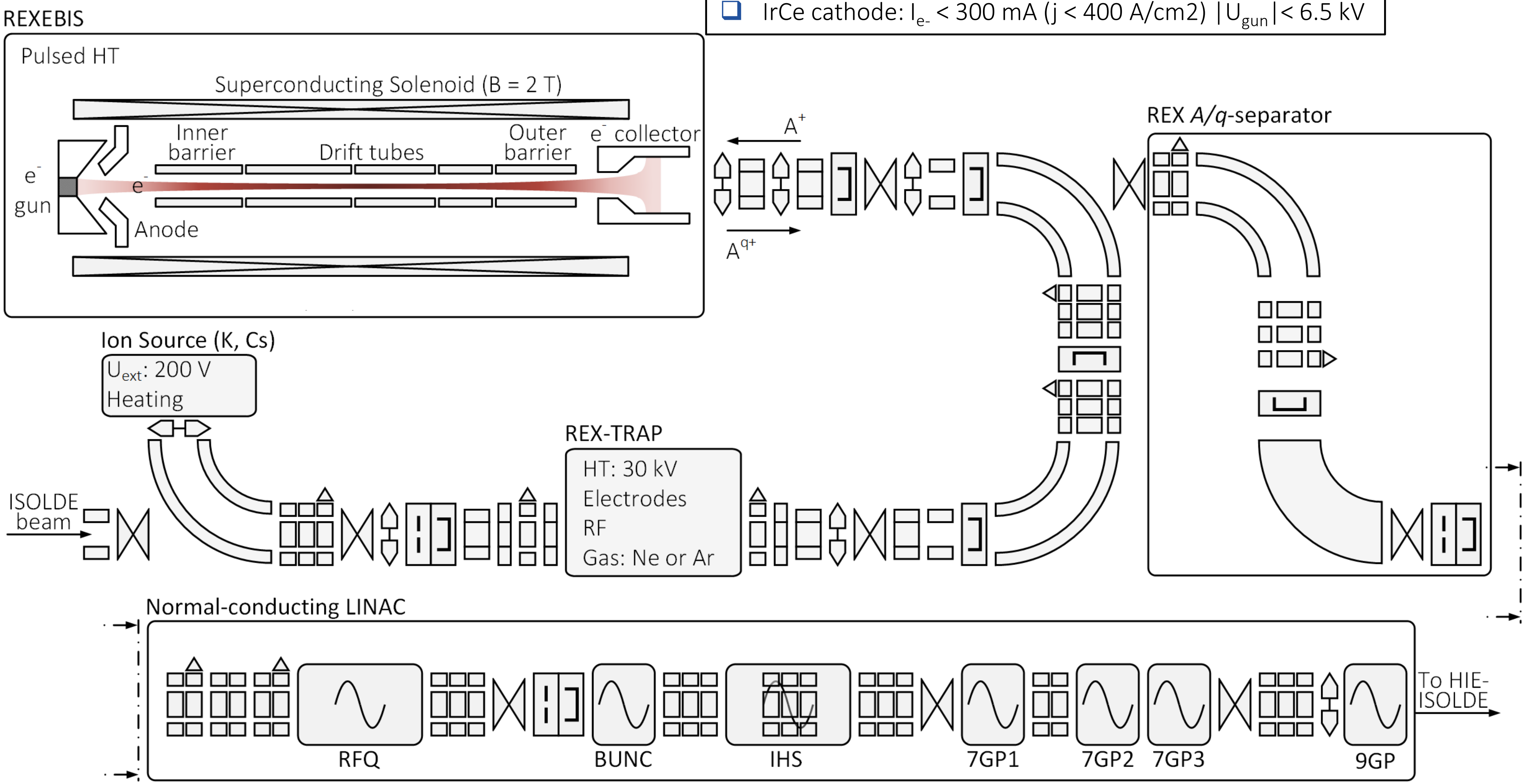

Slow Extraction

Method Regulate the spill of ions over the outer barrier of the EBIS with a constant escape rate: $\int_{V_{t_i}}^{V_{t_{i+1}}} f(U)\,\mathrm{d}U = \frac{\Delta t}{T_p}\int_0^{V_{t_0}} f(U)\,\mathrm{d}U$

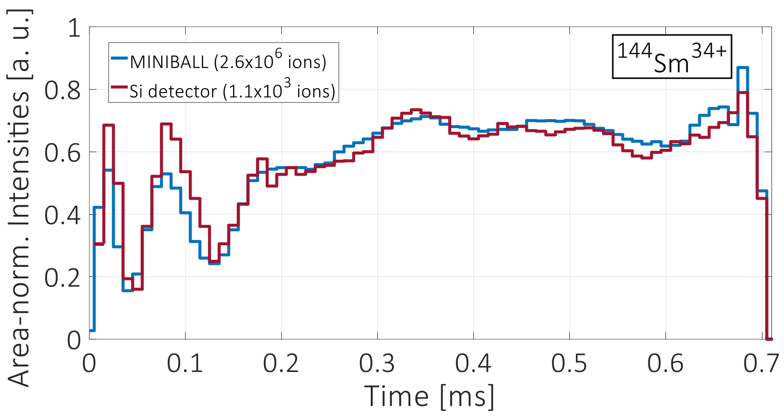

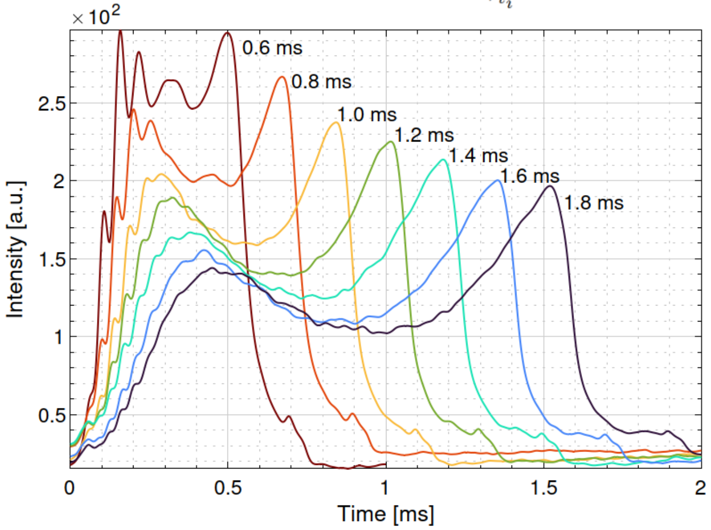

Results Capability to probe and modulate the time structure of very low intensity ion beams.

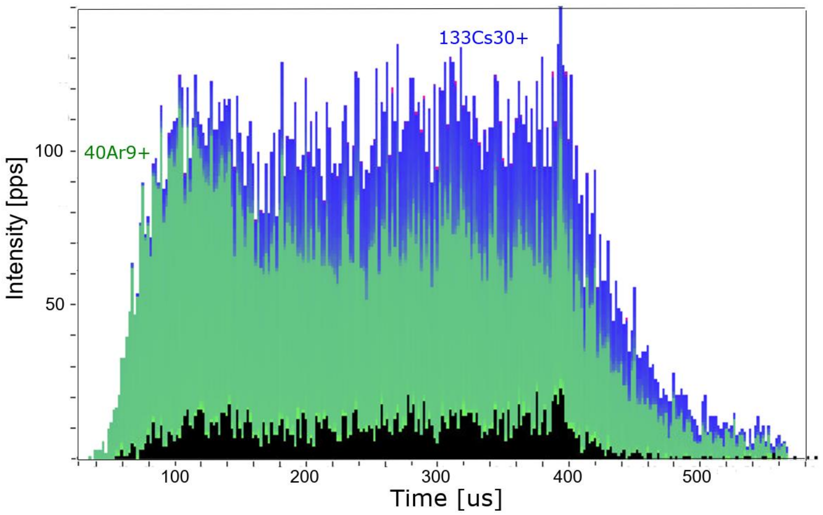

Application Reduction of contamination via delayed extraction of the beam of interest (high CS) ca be improved, notably with larger temperature differences.

"Slow Extraction of Charged Ion Pulses from the REXEBIS", N. Bidault, *et al.,* AIP Conf. Proc. 2011 (2018) 070003.

Axial energy distribution

Technique Variation of REXEBIS extraction potential and monitoring of escaped ions to reconstruct the axial energy distribution.

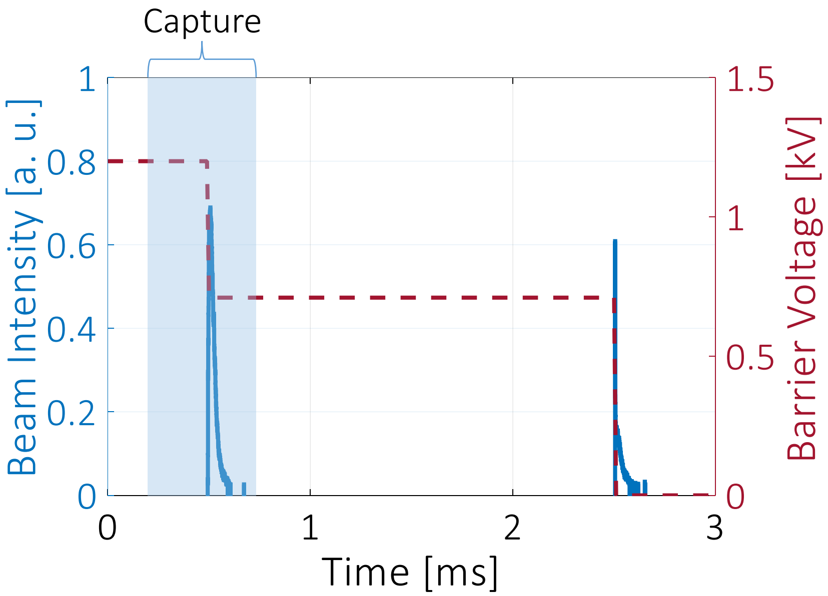

Time-of-Flight of ions measured after the *A/q*-Separator when gating with the outer barrier.

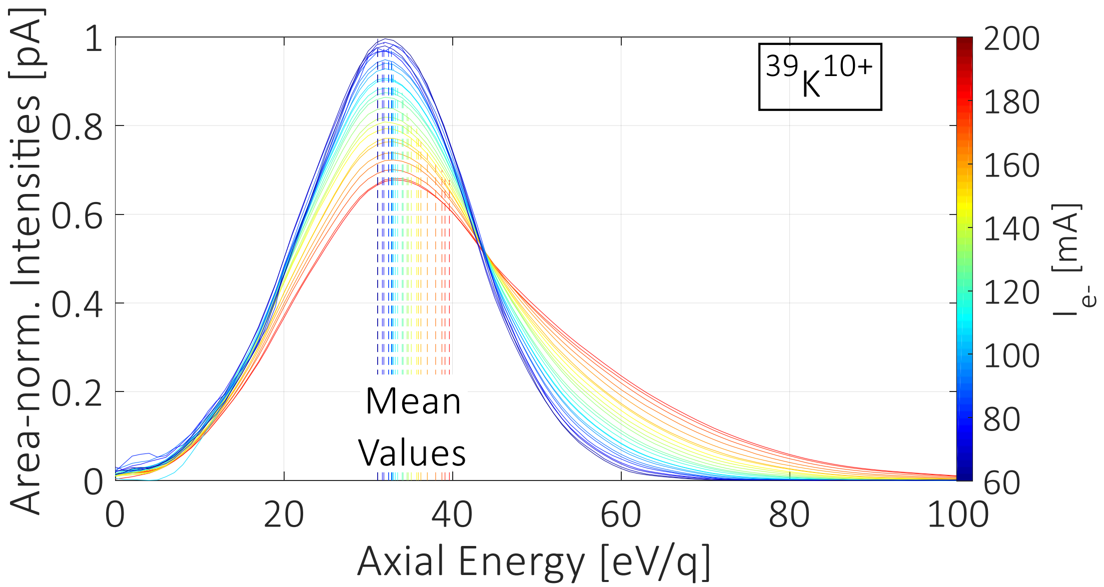

Ionic axial energy distribution measured at REXEBIS extraction, as a function of the electron beam current.

Assumption Ion energy distributions are Maxwell-Boltzmann with 5 degrees of freedom: $f_i(E_\phi)\mathrm{d}E_\phi = \frac{4}{3}N_i\sqrt{\frac{1}{\pi}}(E_\phi)^{3/2}\left(\frac{1}{k_BT_i}\right)^{5/2}\exp\left(\frac{-E_\phi}{k_BT_i}\right)\mathrm{d}E_\phi$

Energy dynamics

$$\frac{\mathrm{d}k_BT_i}{\mathrm{d}t} = \left(\frac{\mathrm{d}k_BT_i}{\mathrm{d}t}\right)^{\text{Spitzer}} + \left(\frac{\mathrm{d}k_BT_i}{\mathrm{d}t}\right)^{\text{Ionisation}} + \sum_j\left(\frac{\mathrm{d}k_BT_i}{\mathrm{d}t}\right)_j^{\text{Transfer}} - \left(\frac{\mathrm{d}k_BT_i}{\mathrm{d}t}\right)^{\text{Escape}}$$

EBISIM code: Charge state and energy dynamics

EBISIM package collection of tools for simulating the evolution of the charge state distribution inside an Electron Beam Ion Source / Trap (EBIS/T) using Python. GitHub (https://github.com/HPLegion/ebisim#readme). Developed by Hannes Pahl (CERN).

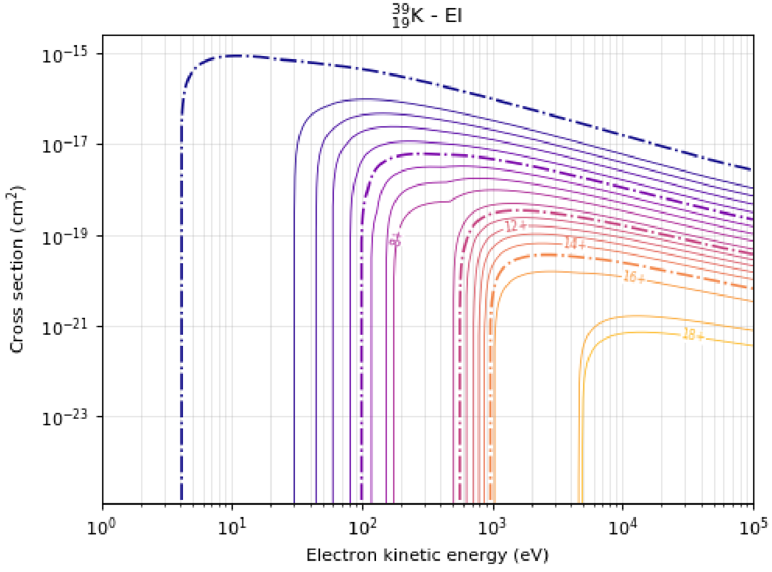

Figure Electron impact cross sections

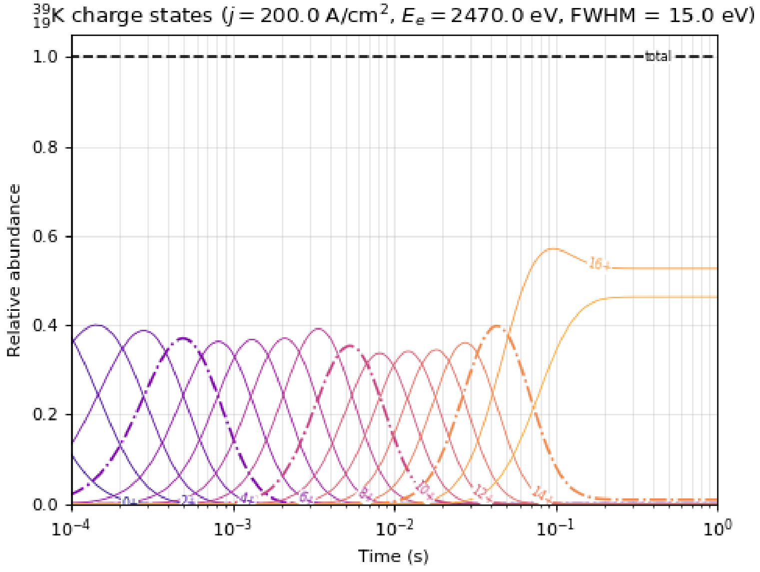

Figure Charge state distribution versus breeding time

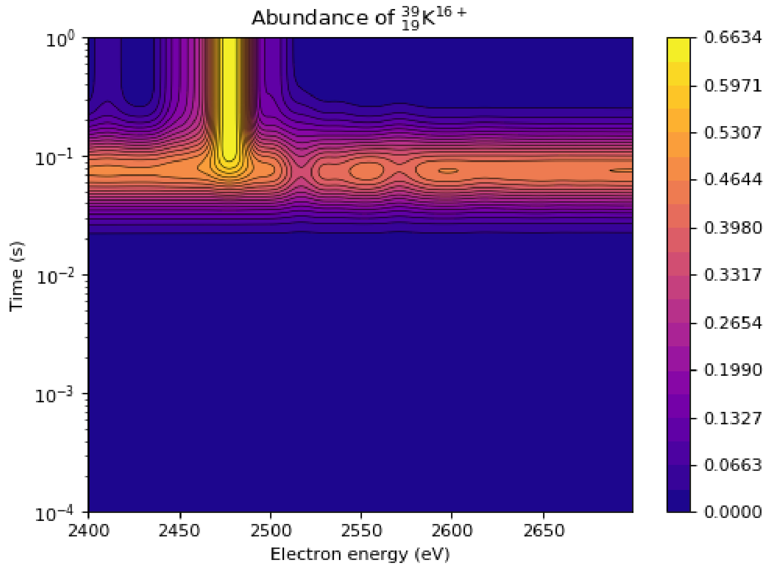

Figure Energy-scan across DR resonances.

Charge dynamics

$$\frac{\mathrm{d}N_q}{\mathrm{d}t} = \frac{j_e}{e} f_{i,e} \left(N_{q-1}\sigma_{q-1}^{\mathrm{EI}} - N_q\sigma_q^{\mathrm{EI}} + N_{q+1}\sigma_{q+1}^{\mathrm{RR}} - N_q\sigma_q^{\mathrm{RR}} + N_{q+1}\sigma_{q+1}^{\mathrm{DR}} - N_q\sigma_q^{\mathrm{DR}} \right) + \sum_j f_{i,j}(n_j \bar{v}_{q+1} N_{q+1}\sigma_{q+1}^{\mathrm{CX}} - n_j \bar{v}_q N_q \sigma_q^{\mathrm{CX}}) + N_q R_q^{\mathrm{esc}} + N_q^{\mathrm{source}}$$

EBIS plasma: Dielectronic recombination process

Experimental setup $^{39}K^{q}$ for q = 13…17 @ 4 keV/u . RR = 1 Hz; Breeding time = 995 ms; I_{e-} = 50 mA. Potential use for charge state selectivity

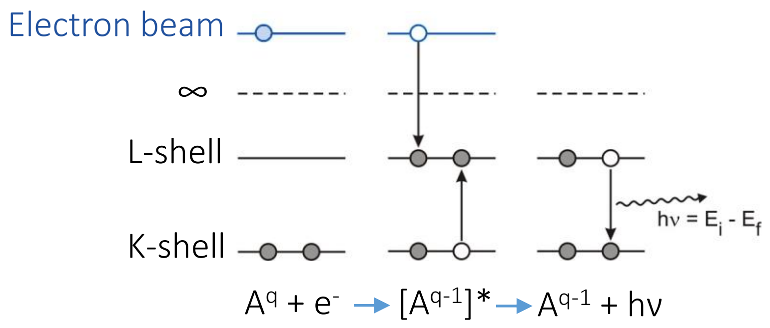

Figures of merit:

- ❑ Effective electron beam current density
- ❑ Space charge energy correction
- ❑ Electron energy spread

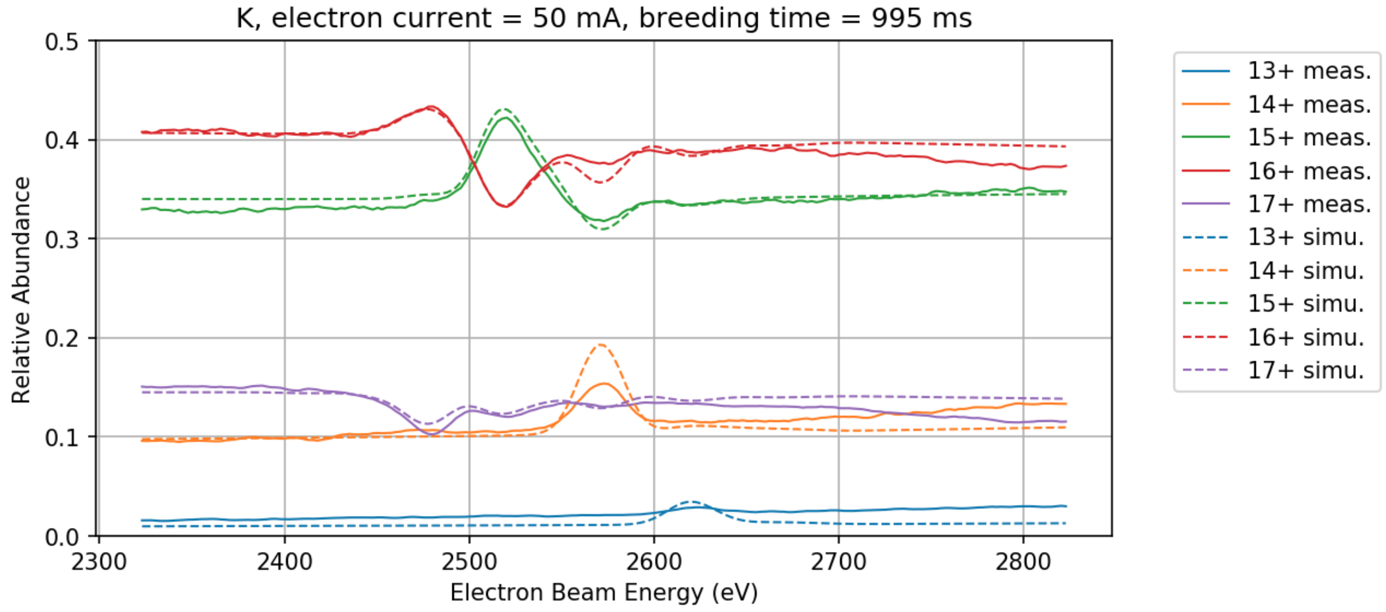

Measurement of the charge state relative abundancies and comparison with EBISIM code featuring dielectric recombination effects in REXEBIS.

Space charge potential inside an EBIS

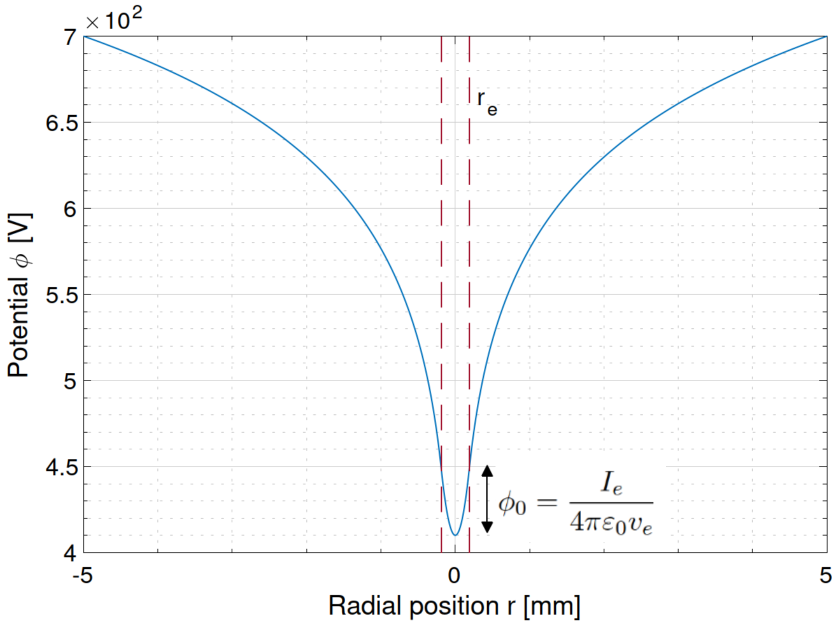

Space charge potential from the electron beam only.

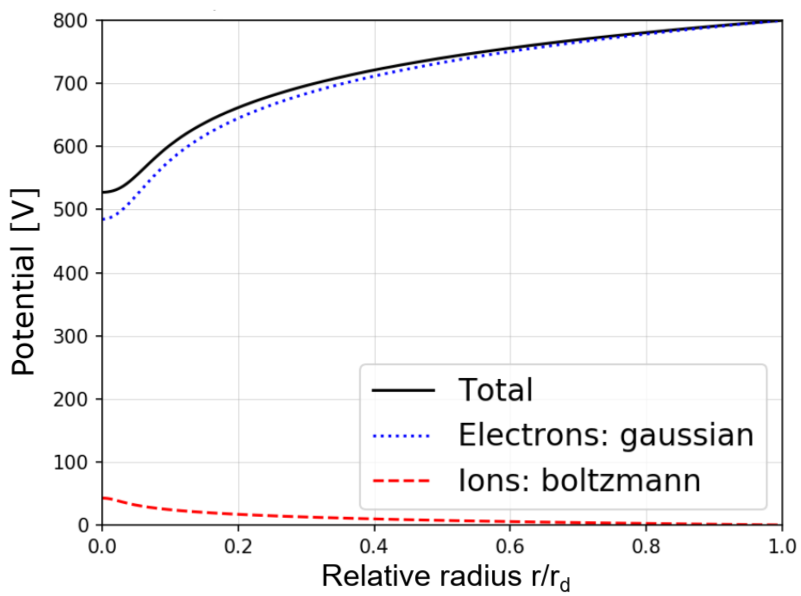

Space charge potential including ion beam compensation.

Regime of convergence

$$N_i(r > r_e) \propto \int_{r_e}^{+\infty} n_i(r) r \mathrm{d}r$$
$$\propto \int_{r_e}^{+\infty} r^{1-2Q_i\Phi_0/(k_B T_i)} \mathrm{d}r$$

Use Riemann criteria.

With uniform e-beam:

$$\phi(r) = U_t - \phi_0 \cdot \begin{cases} \left(2\ln\frac{r_t}{r_e} - \frac{r^2}{r_e^2} + 1\right) & , |r| \le r_e \\ 2\ln\frac{r_t}{|r|} & , |r| > r_e \end{cases}$$

Gauss law:

$$\nabla \cdot \mathbf{E} = \frac{\partial}{\partial r}\left(r\frac{\partial \phi(r)}{\partial r}\right) = \frac{e}{\varepsilon_0}\left(n_e(r) - \sum_i \sum_q q_i n_{i,q}(r)\right)$$

Using Boltzmann distribution:

$$n_i(r, t = \infty) = n_i(0) \exp\left(-\frac{Q_i \phi(r)}{k_B T_i}\right)$$

Beam properties at extraction from an EBIS

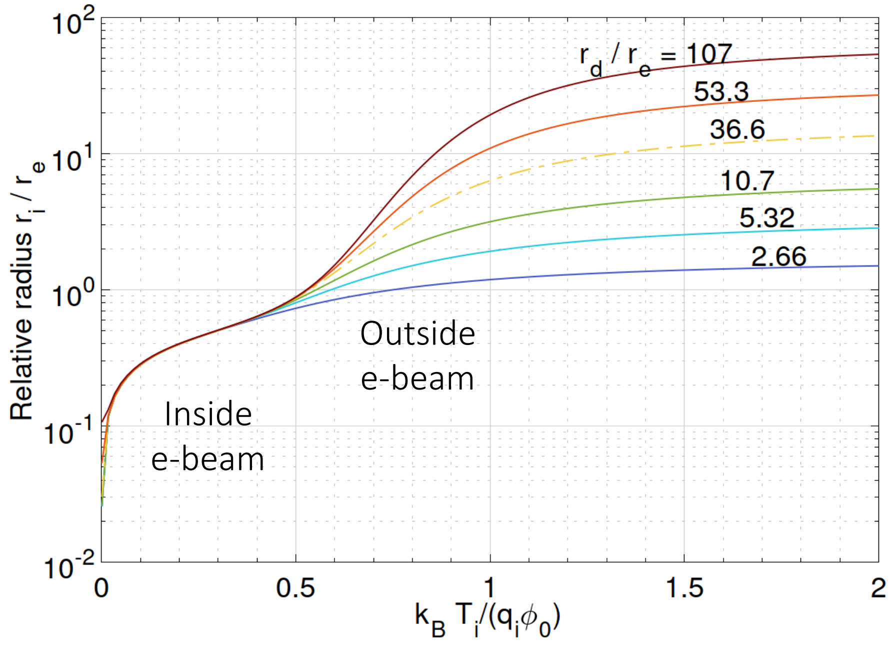

Average radius of the ion cloud versus temperature.

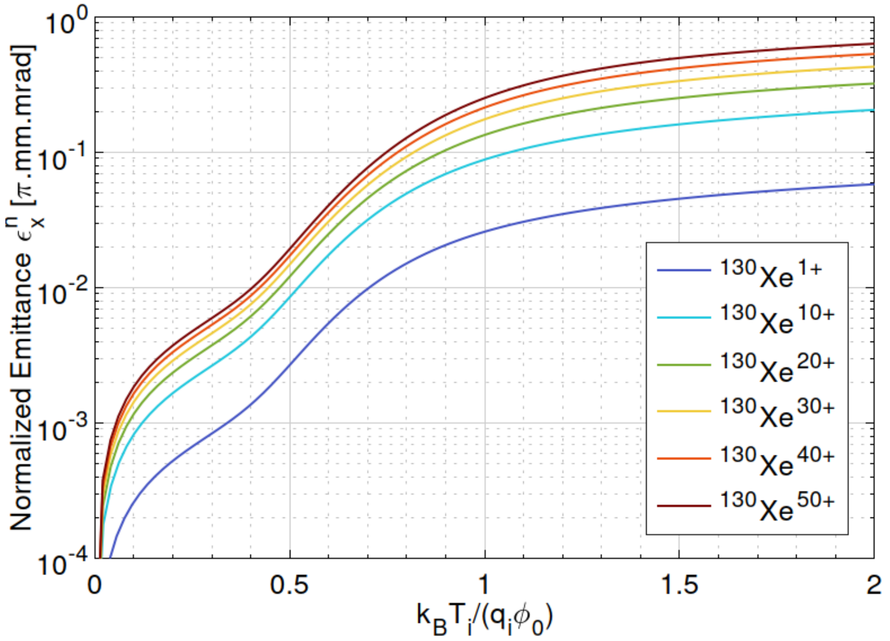

Normalized emittance of extracted beam in a field free region.

Ion cloud characteristic radii:

$$r_i = \int_{\mathbb{R}_+} r^2 n_i(r)\mathrm{d}r \qquad r_i^{\mathrm{rms}} = \sqrt{\int_{\mathbb{R}_+} r^3 n_i(r)\mathrm{d}r}$$

Deduction of the overlap factor between electron and ion distributions.

Transverse emittance in EBIS (Cartesian coordinates):

$$\varepsilon_x = \sqrt{\frac{k_B T_i}{2 m_i v_z^2}\left[(r_i^{\mathrm{rms}})^2 - \frac{r_i^2}{\pi}\right]}$$

Emittance in field free region, from canonical momentum conservation,

$$\varepsilon_x^2(B=0) = \varepsilon_x^2(B=B_d) + \frac{Q_i^2 B_d^2}{16 m_i^2 v_z^2}(r_i^{\mathrm{rms}})^4$$

Measurement of the overlap factor

Experimental setup Neutral gas injection of [129]Xe. Electron beam with a current of 200 mA and energy about 6 keV. Axial energy scans with varying breeding time.

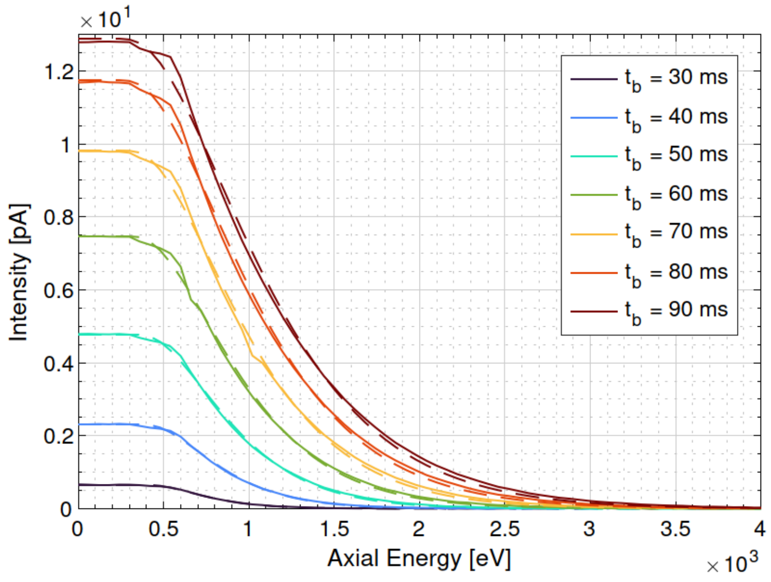

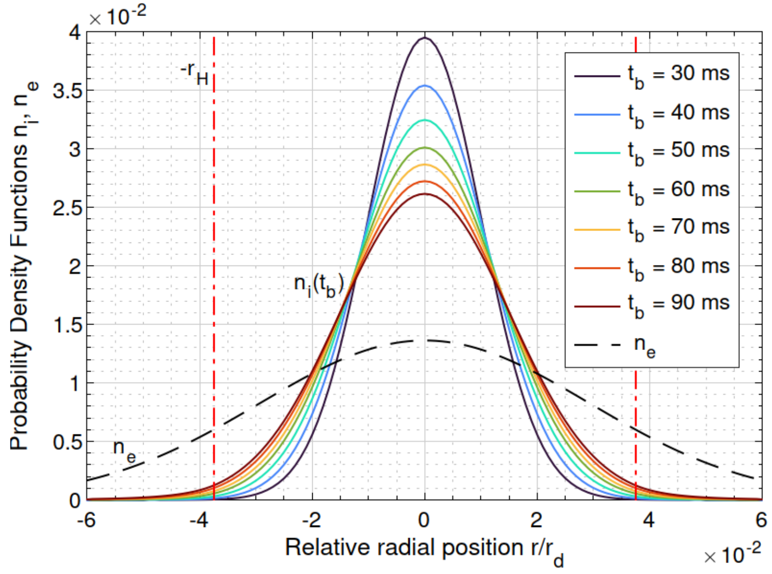

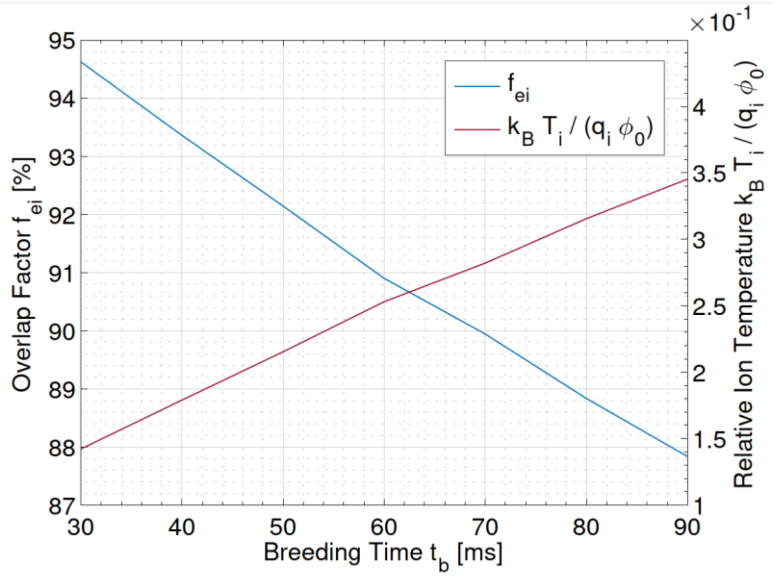

Method

Fitting of three free parameters, using the lower gamma incomplete function:

$$f(U) = I_0(1 - \gamma\left(\frac{q_i U - E_0}{k_B T_i}, \frac{5}{2}\right))$$

Results

Estimate of the ion temperature.
Deduce the ion radial distribution.
Calculate the overlap factor.

Conclusion

The ion cloud remains confined within the electron beam.
Heating rate:
- Measured: 3.5 keV/s
- From Landau-Spitzer: 2.4 keV/s

Estimation of the effective electron current density

Objective Estimate the effective electron current density j_{eff}, when comparing the measured charge state distributions with the EBISIM code.

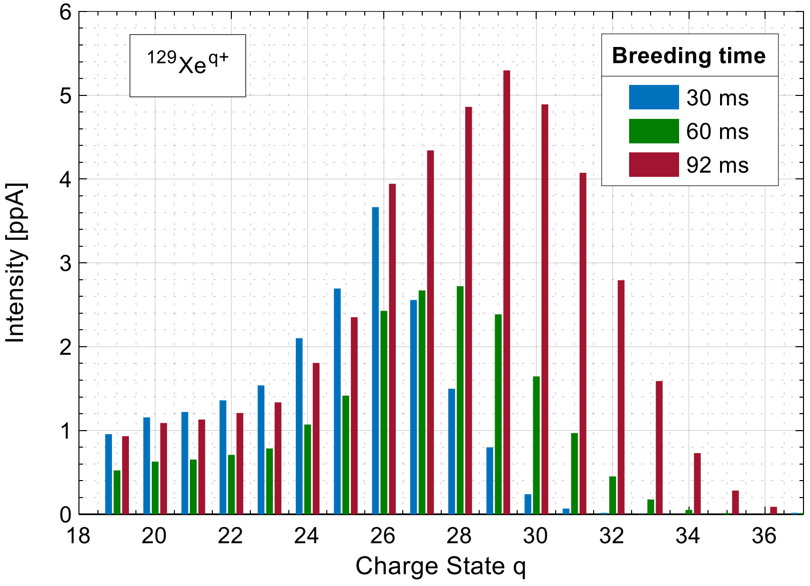

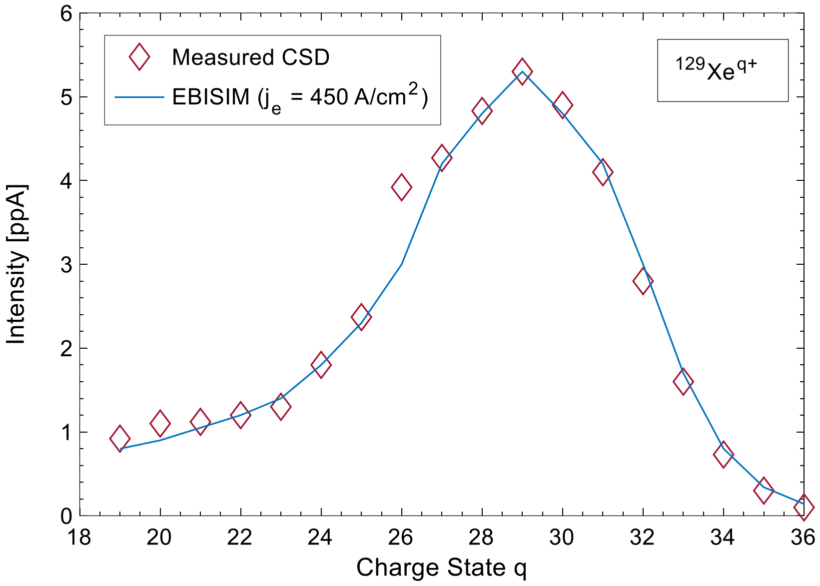

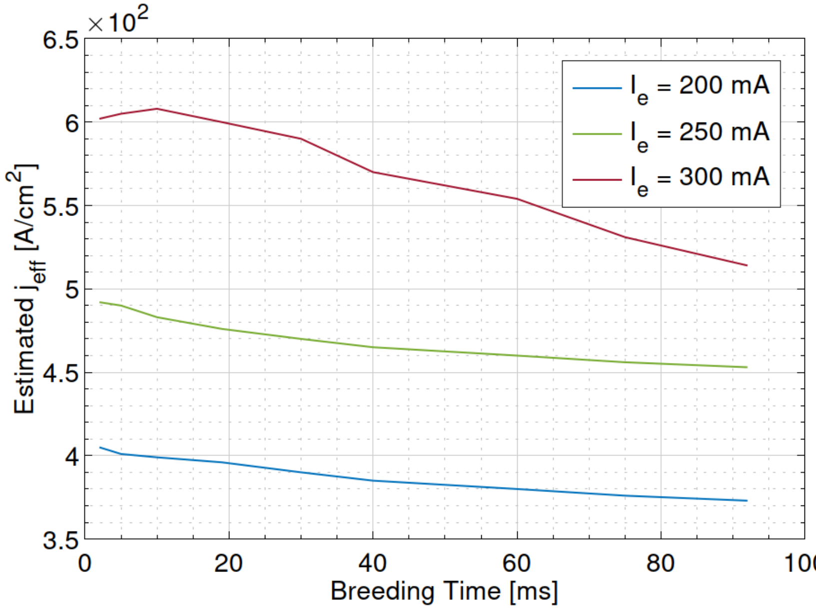

Method

Measurement of the charge state distribution of $^{129}Xe^{q+}$ for different breeding time.

Result

Deduce the effective electron current density from a least-square minimization between the EBISIM code and the measurements.

Conclusion

- j_{eff} = 600 A/cm^2 for I_{e-} = 300 mA.
- j_{eff} = 400 A/cm^2 for I_{e-} = 200 mA.

The decreasing trend can be explained with the reduction of the overlap factor.

Beam Quality

Beam Intensity Optimization

Slow extraction

Charge-breeding performances

Beam Purity

EBIS partial pressures

Rare contaminants

Transverse properties

Quadrupole-scan

Trace space reconstruction

Longitudinal properties

Beam energy distribution

Bunch structure

Abundant contamination

Technique Variation of REX A/q-Separator magnet, monitoring of current passing through slit on Faraday cup.

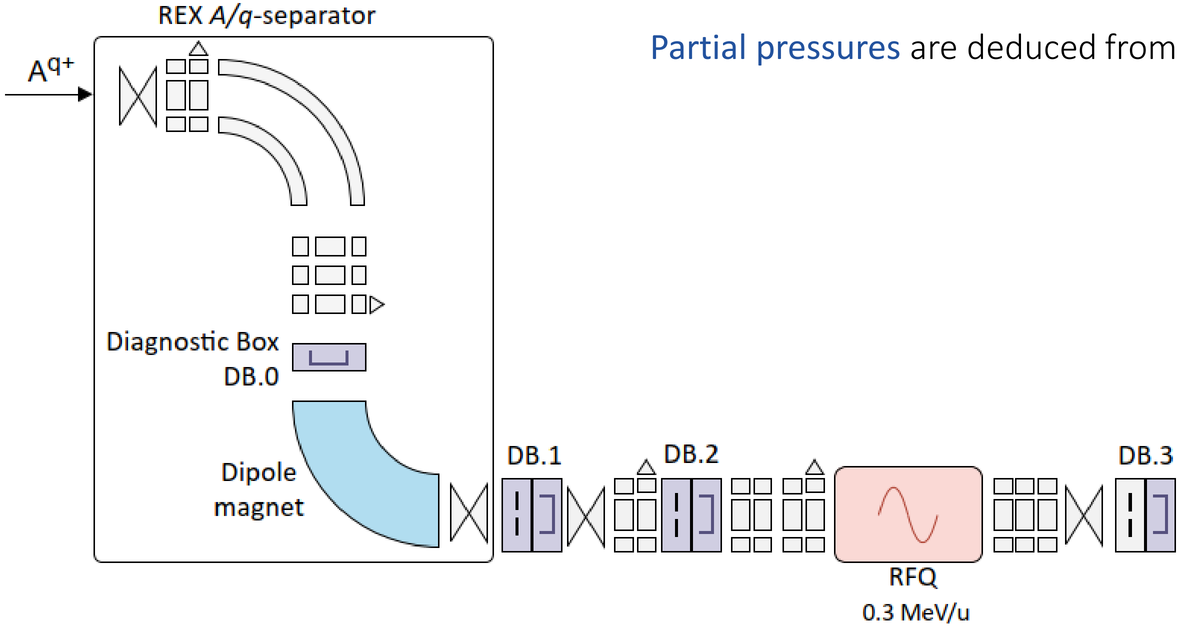

Partial pressures are deduced from the simplified model: $\frac{\mathrm{d}N_q}{\mathrm{d}t} \simeq \frac{Ie}{e}\frac{p}{k_B T_i} L_d \left[f_{q-1}\sigma^{\mathrm{EI}}_{q-1} - f_q\left(\sigma^{\mathrm{EI}}_q + \sigma^{\mathrm{RR}}_q\right) + f_{q+1}\sigma^{\mathrm{RR}}_{q+1}\right]$

Element	Density [mm^{-3}]	Pressure [mbar]
Nitrogen	4.0 .10^{7}	1.6 .10 $^{-10}$
Oxygen	1.5 .10^{7}	6.0 .10 $^{-11}$
Carbon	6.0 .10^{7}	2.4 .10 $^{-10}$
Neon	2.0 .10^{6}	8.0 .10 $^{-12}$
Argon	5.0 .10^{6}	2.0 .10 $^{-11}$

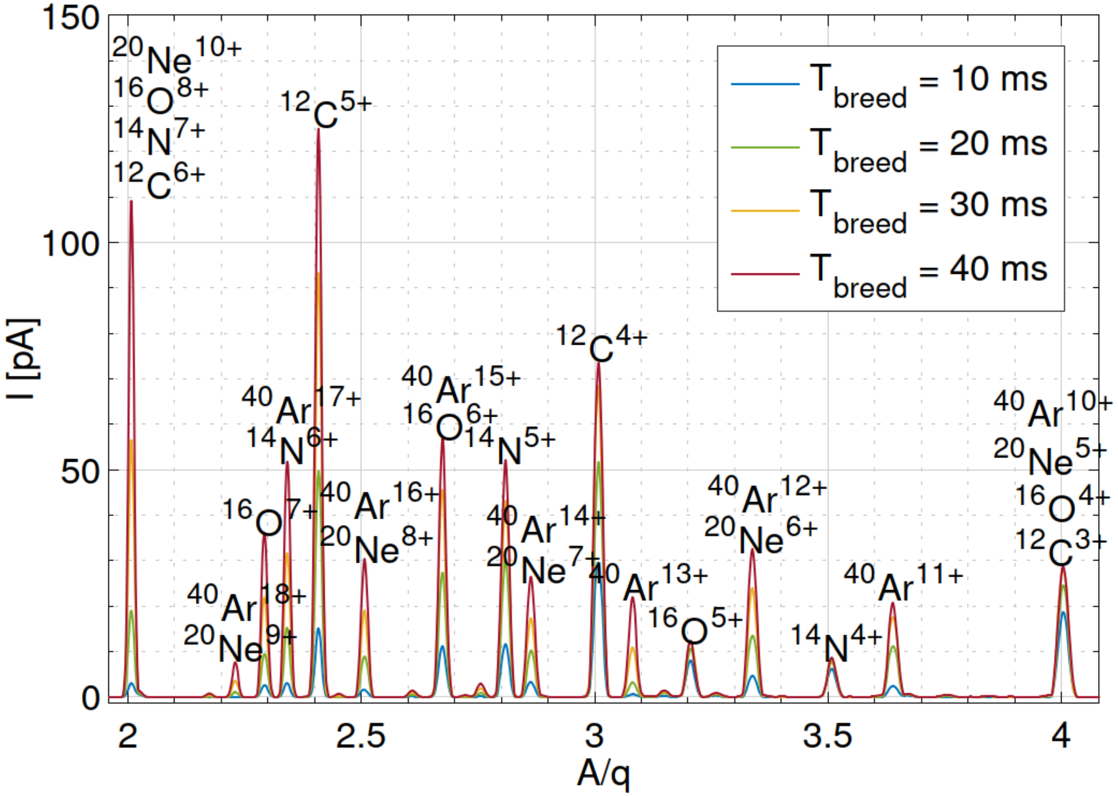

A/q-scan measured with a Faraday cup. I_e = 200 mA, E_e = 6 keV.

From epA to single-ion detection

Technique Instead of varying REX *A/q*-Separator magnet, all necessary beam optics and RF, from REXEBIS to the Si detector, are scaled for each A/q step.

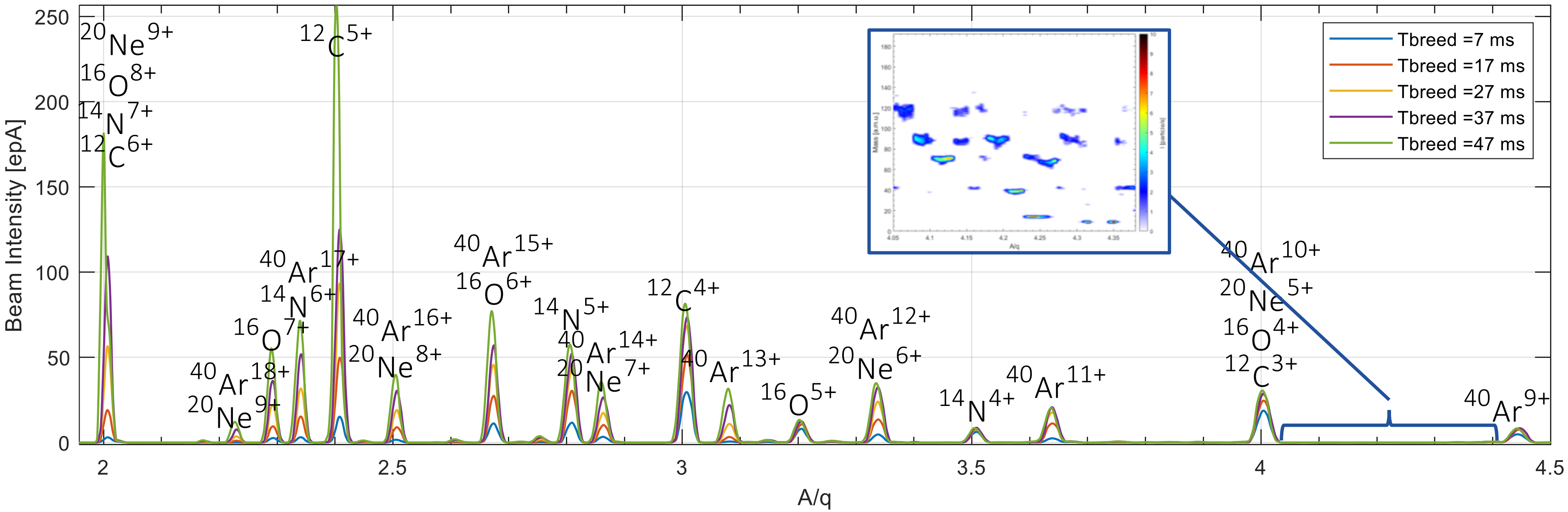

Objective Anticipate on the beam purity and probe *A/q*-areas where Faraday cups do not allow for identification

Experimental setup in 2020, using non-adiabatic gun with IrCe cathode at higher electron beam density:

- Confirmation of the capability to probe rare contaminants.
- Residual gas ions were accelerated through the RFQ and acquired on a large Si detector installed directly afterward.
- Intensities are representative of reality.

Rare contaminants

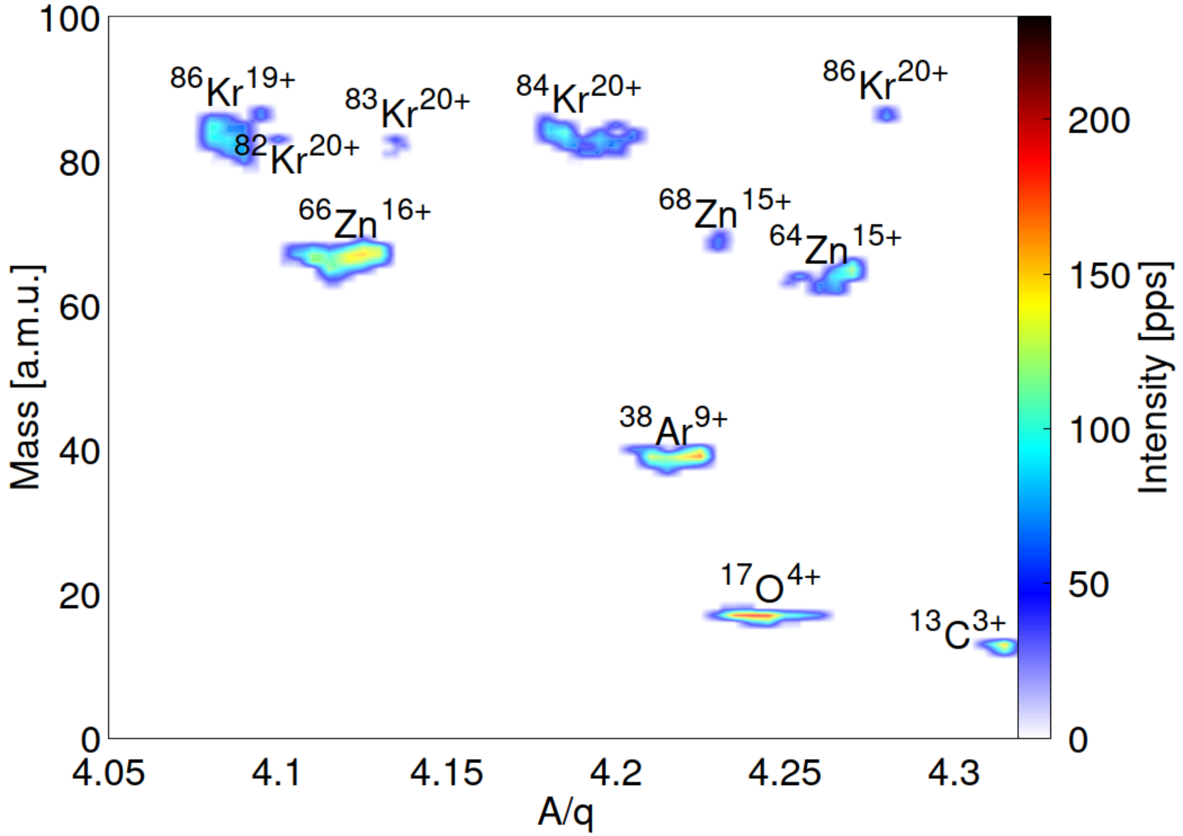

Method A/q-scan measured with a silicon detector. I_e = 200 mA, E_e = 6 keV.

Application Investigation on the presence of Ir or Ce from the electron gun cathode using the silicon detector energy histograms.

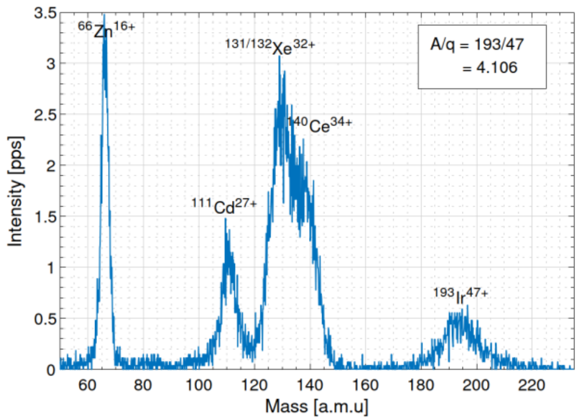

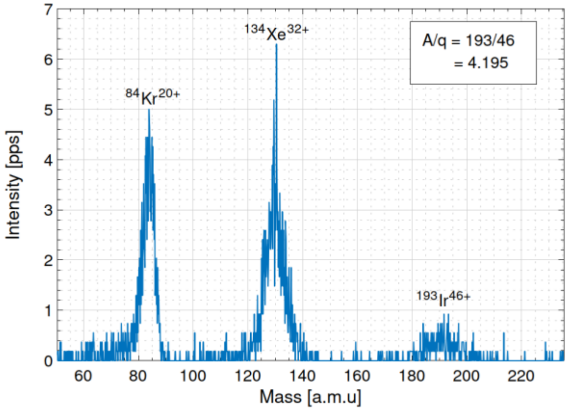

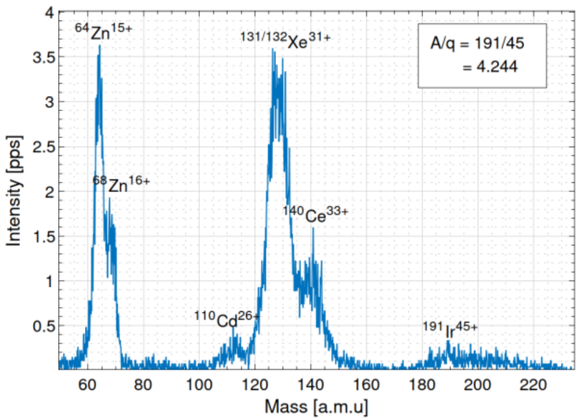

Results

- Correlation with neighboring CS
- Poor energy resolution
- Negligible Ir/Ce contamination
- Cathode can be used

Beam Quality

Beam Intensity Optimization

Slow extraction

Charge-breeding performances

Beam Purity

EBIS partial pressures

Rare contaminants

Transverse properties

Quadrupole-scan

Trace space reconstruction

Longitudinal properties

Beam energy distribution

Bunch structure

HIE-ISOLDE

REX LINAC basic parameters

f = 101.28 MHz
Four-rod λ/2 RFQ and Buncher
IH-structure
Three 7-Gap resonators
9-Gap resonator (f = 202.56 MHz)

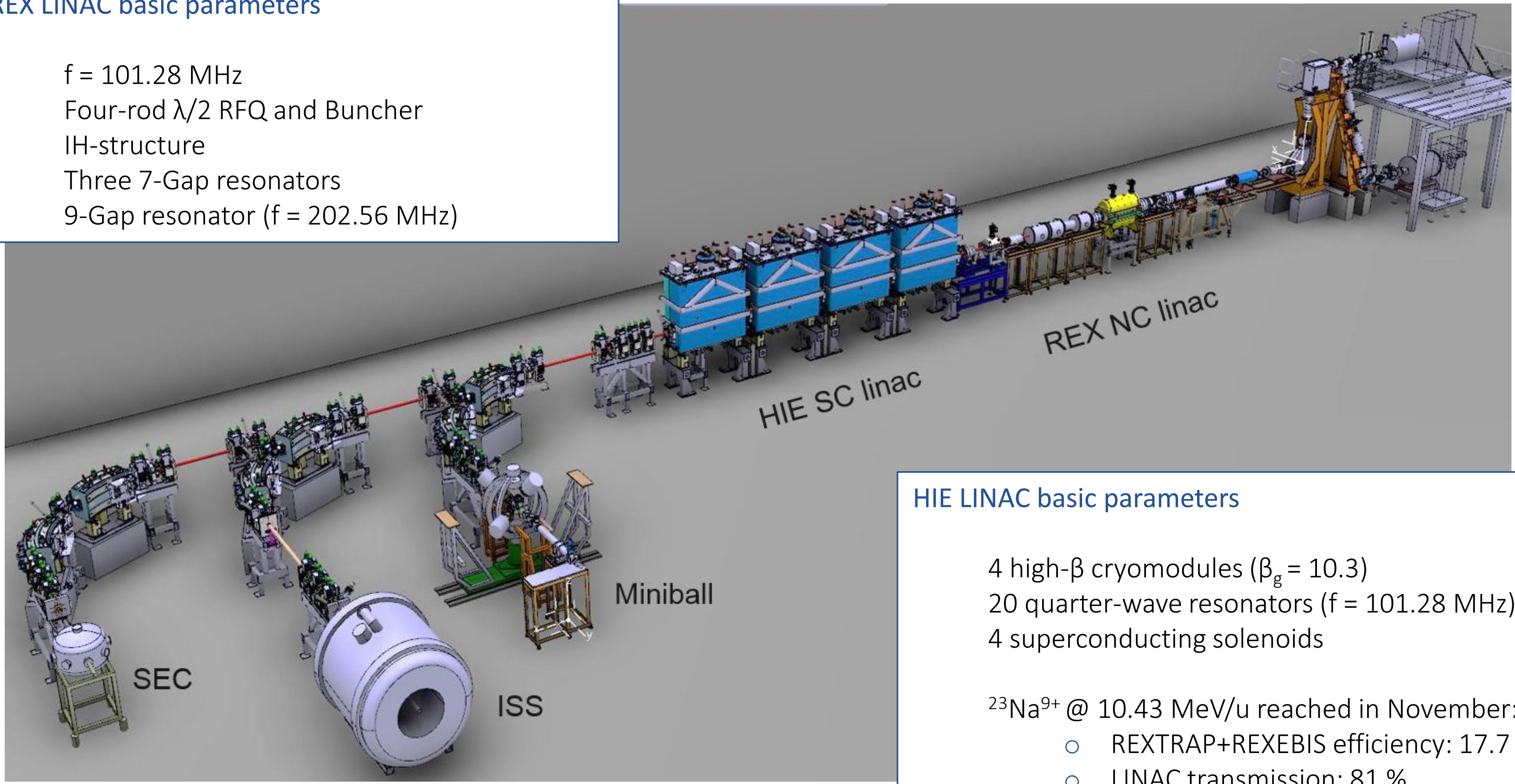

HIE LINAC basic parameters

4 high-β cryomodules (β_g = 10.3)
20 quarter-wave resonators (f = 101.28 MHz)
4 superconducting solenoids

$^{23}Na^{9+}$ @ 10.43 MeV/u reached in November:

- REXTRAP+REXEBIS efficiency: 17.7 %
- LINAC transmission: 81 %

HIE-ISOLDE: Transverse beam profiles at low intensity

Method

- Measurement of transverse beam profiles at the same location, with a Faraday cup for pA current range or a silicon detector below 1 fA.
- Bias and exclusion (threshold) analysis.

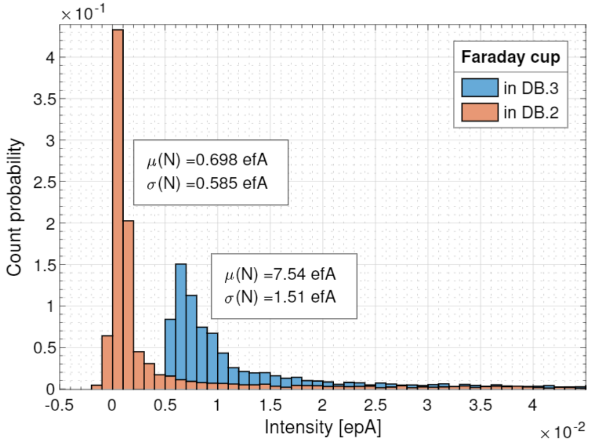

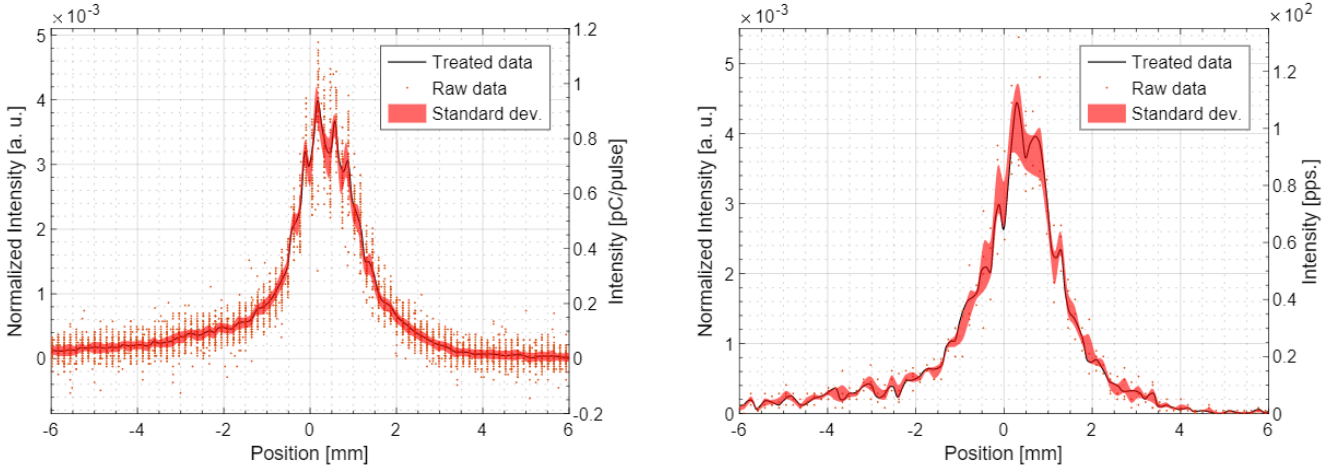

Faraday cup (left) and silicon detector (right) beam profile measurements

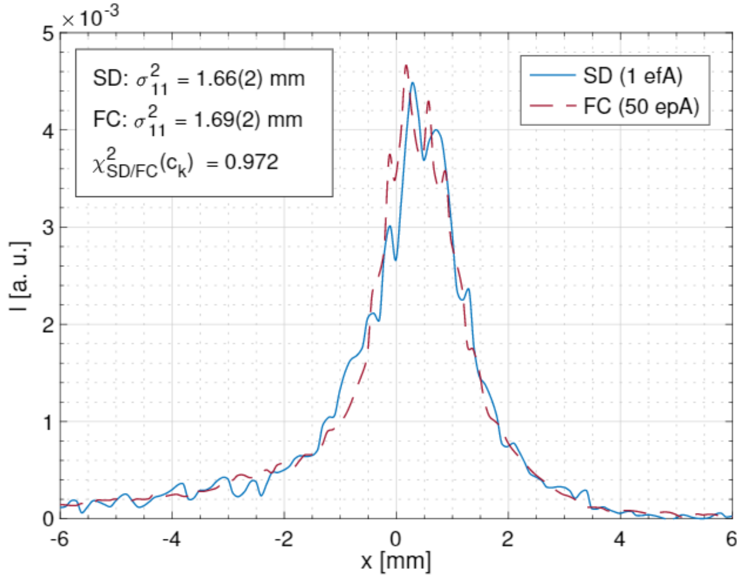

Result Capability to measure transverse profiles of very low intensity ion beams.

HIE-ISOLDE: Transverse beam properties characterization

Experimental setup $^{39}K^{10+}$ @ 3.82 MeV/u, thin-slits and quadrupoles are used to probe the tranvserse phase-space for two ranges of intensity.

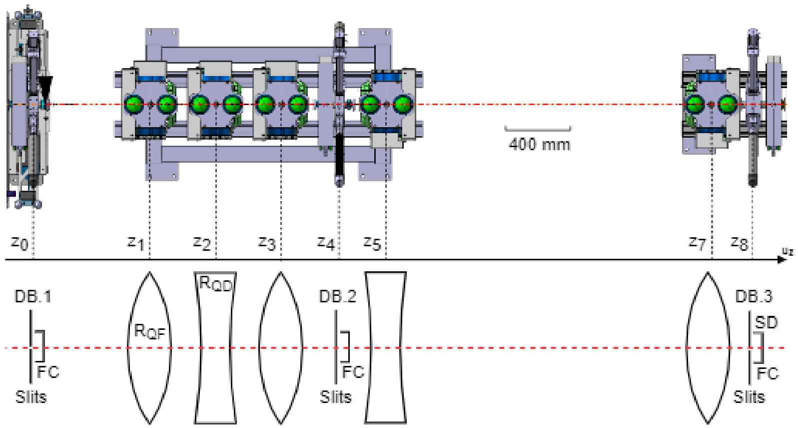

Treatment when using Faraday cup as beam collector

Deduce a threshold from the evolution of the second derivatives of the Twiss paramaters.

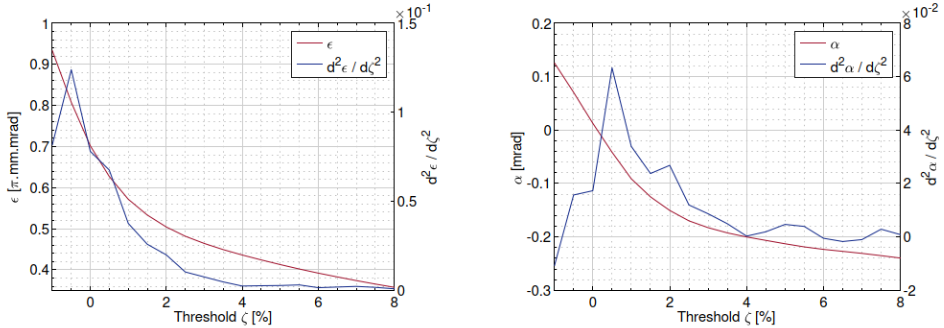

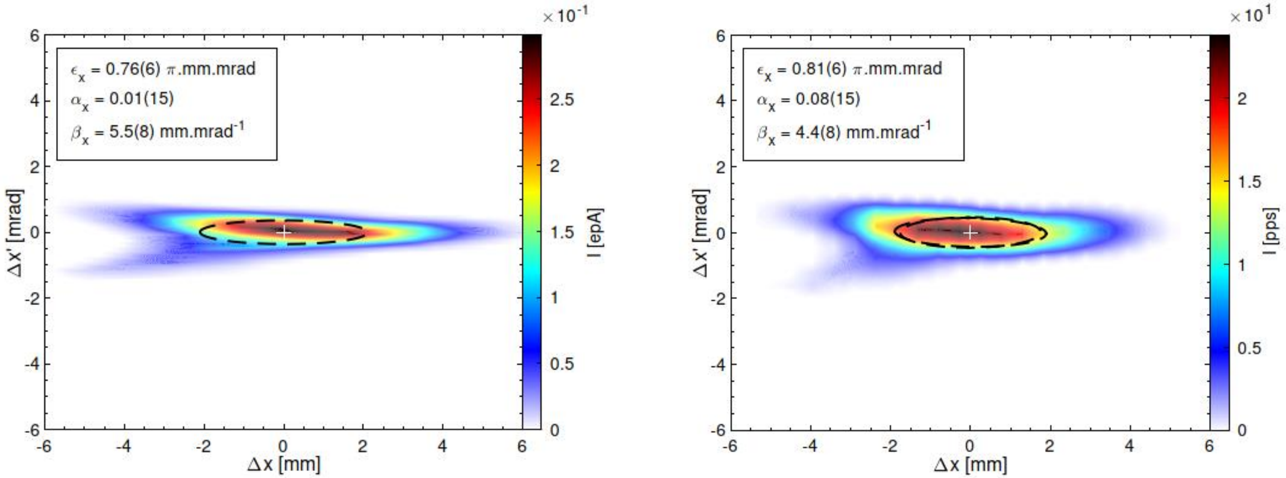

Left: Double-slit scan using Faraday cup (>10 epA). Right: Silicon detector (<1 efA).

Technique

With the double-slit scan, the transverse phase-space is sliced twice. Beamlet acquired via a silicon detector or a Faraday cup.

Result

Validation of the new methodology with very low intensity ion beams. Correlation of the results for the two ranges of intensity.

"Characterization of the transverse properties of very low intensity ion beams at the REX/HIE-ISOLDE LINAC", N. Bidault, *et al.,* NIM-A, in-review.

HIE-ISOLDE: Transverse beam properties characterization

Experimental setup $^{39}K^{10+}$ @ 3.82 MeV/u, thin-slits and quadrupoles are used to probe the tranvserse phase-space for two ranges of intensity.

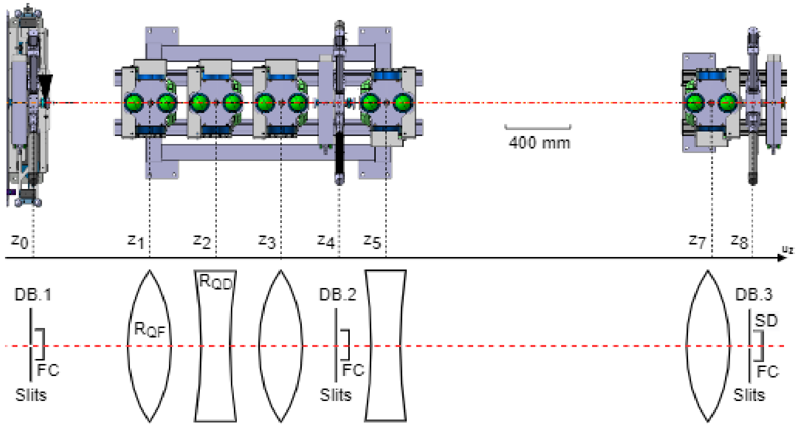

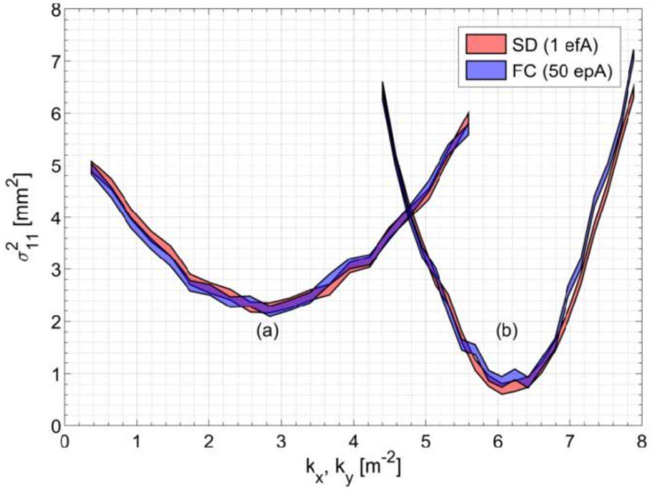

Results

Plane	Parameter	Value SD	Value FC
	ε_x [π.mm.mrad]	0.80(5)	0.82(5)
	α_x	−0.10(15)	0.05(15)
x-plane (a)	β_x [mm.mrad^{-1}]	4.8(5)	5.1(5)
	γ_x [mrad.mm^{-1}]	0.21(3)	0.20(3)
	$\chi^2_{SD/FC}(\sigma^2_{11})$	0.988	
	ε_y [π.mm.mrad]	0.71(5)	0.75(0.5)
	α_y	−0.64(15)	−0.60(15)
y-plane (b)	β_y [mm.mrad^{-1}]	2.4(3)	2.8(3)
	γ_y [mrad.mm^{-1}]	0.25(11)	0.23(9)
	$\chi^2_{SD/FC}(\sigma^2_{11})$	0.984	

Method With the quadrupole scan the tranvserse phase-space rorated and sliced once.

Tomography
Reconstruction of the trace space from the quadrupole-scan.

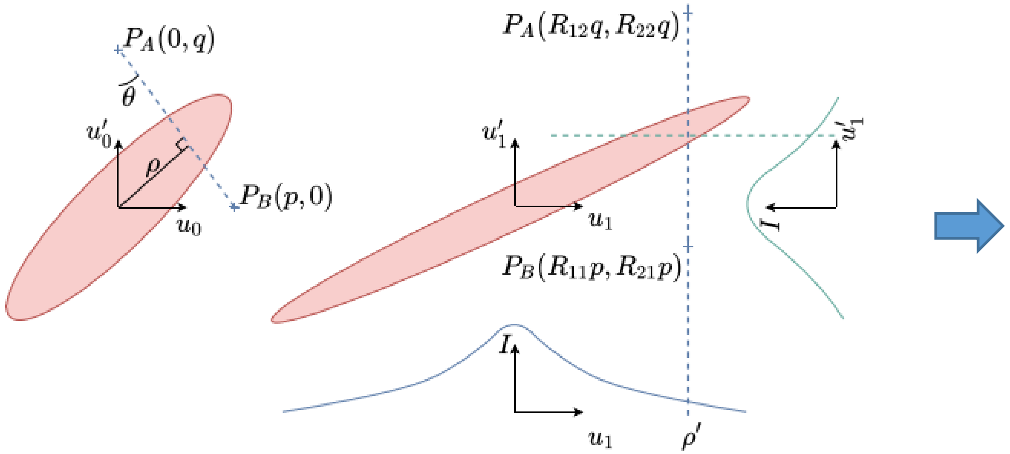

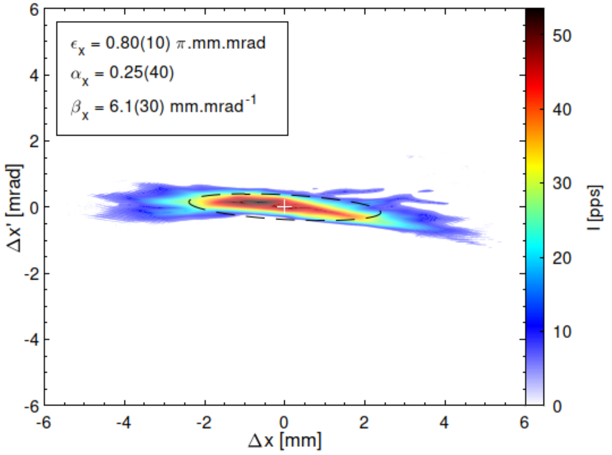

Beam Quality

Beam Intensity Optimization

Slow extraction

Charge-breeding performances

Beam Purity

EBIS partial pressures

Rare contaminants

Transverse properties

Quadrupole-scan

Trace space reconstruction

Longitudinal properties

Beam energy distribution

Bunch structure

HIE-ISOLDE: Beam energy distribution measurement

Technique Use of an HEBT dipole as energy-spectrometer and three vertical slits. Acquisition of the beamlet current with a silicon detector.

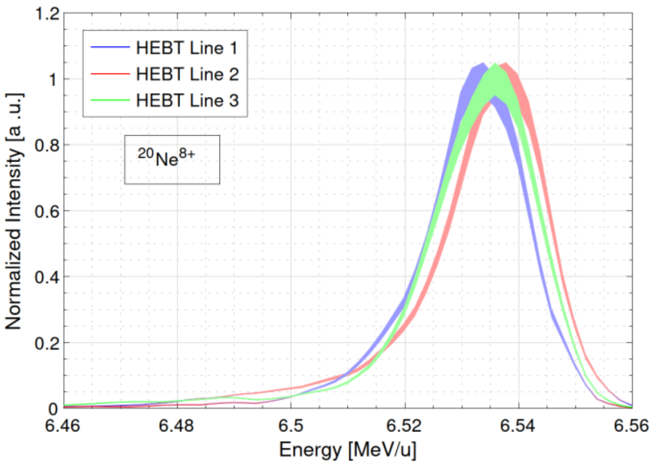

Measurements using the three HEBT dipoles confirmed to be similar.

The energy spread derived is overestimated depending on the beam transverse emittance and the spacing between the 1-mm vertical slits.

Proven capability to measure the energy distribution of very low intensity ion beams.

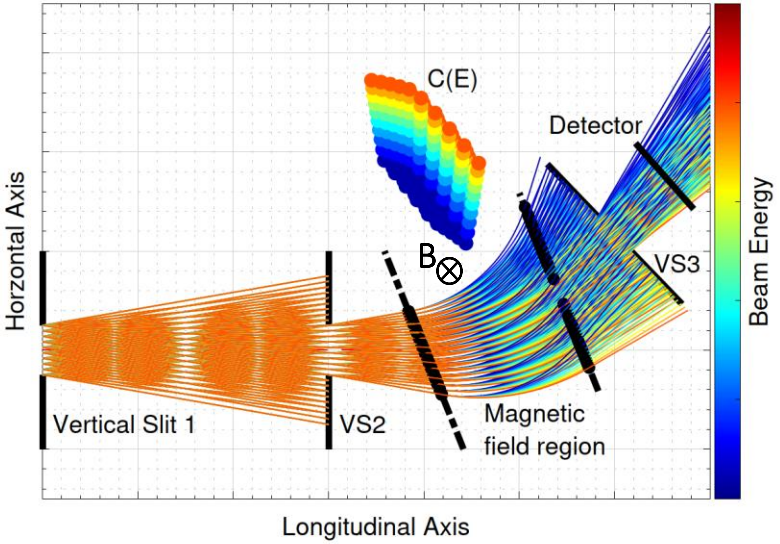

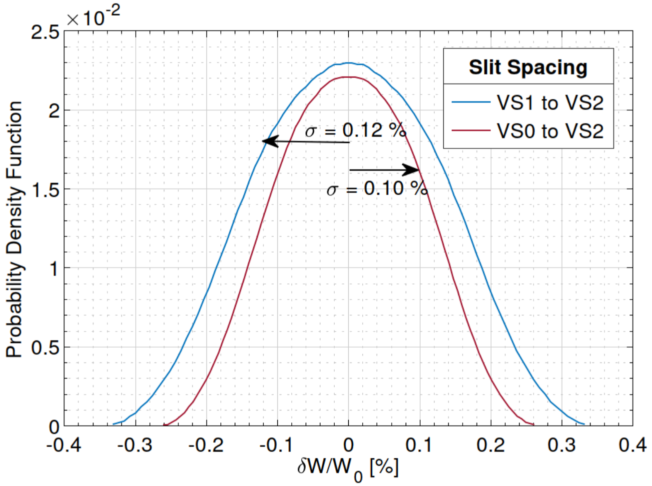

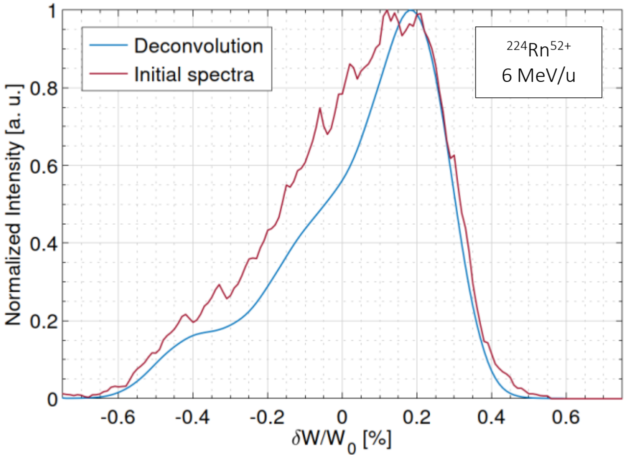

Method Estimate the inherent spread introduced by the thin slits in the measurement channel and deconvolute the energy distribution measured from a RIB.

HIE-ISOLDE: Longitudinal phase-space characterization

$$\mathscr{E}(z_0) : \gamma_z(\Delta t)^2 + 2\alpha_z \Delta t \Delta W/A + \beta_z(\Delta W/A)^2 = \varepsilon_z$$

$$\mathcal{R}_{\mathrm{RF}}(E_0) = \begin{pmatrix} 1 & 0 \\ 1 & -2\pi f \frac{q}{A} E_0 T L_a \sin(\varphi_s) \end{pmatrix}$$

$$\mathcal{R}_{\mathrm{D}}(L) = \begin{pmatrix} 1 & \frac{-AL}{\beta\gamma(\gamma+1)cW} \\ 0 & 1 \end{pmatrix}$$

$$\boldsymbol{\sigma}(z_1) = \boldsymbol{\mathcal{R}} \cdot \boldsymbol{\sigma}(z_0) \cdot^t \boldsymbol{\mathcal{R}}$$

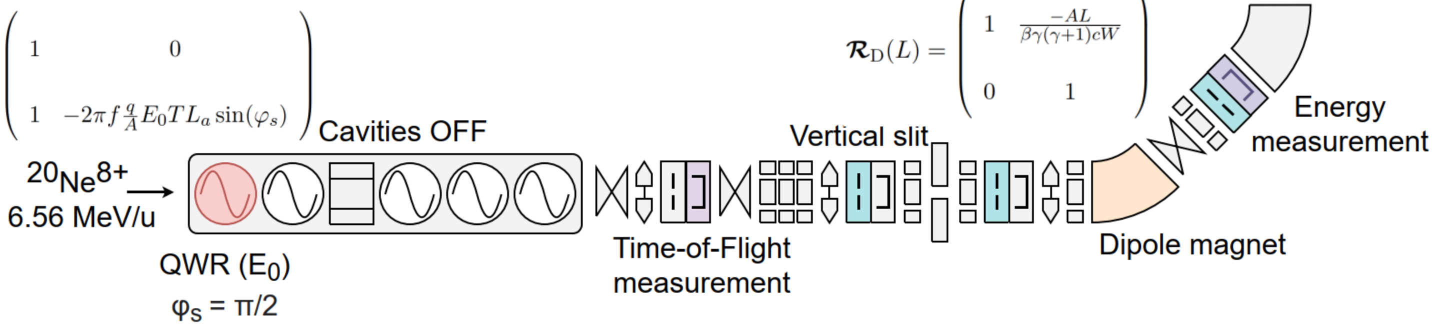

Experimental setup $^{20}Ne^{8+}$ @ 6.64 MeV/u, 10 superconducting cavities (SCC) at nominal accelerating phase, 1 SCC acting as a buncher at zero-crossing phase.

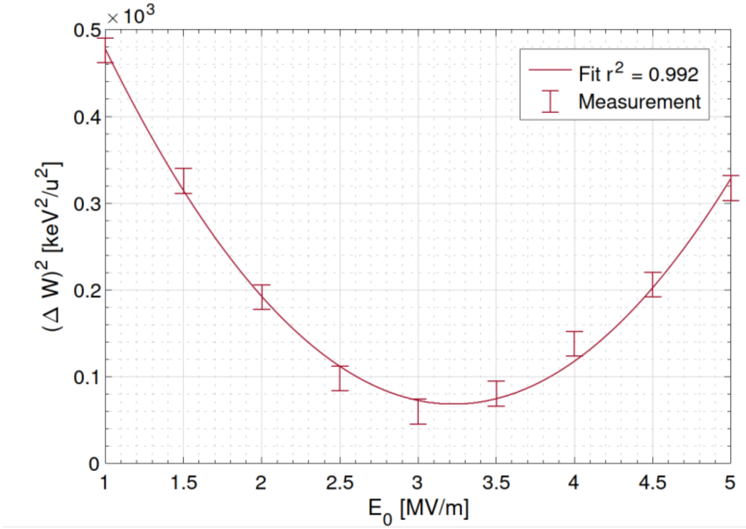

Method Energy spread measurement.

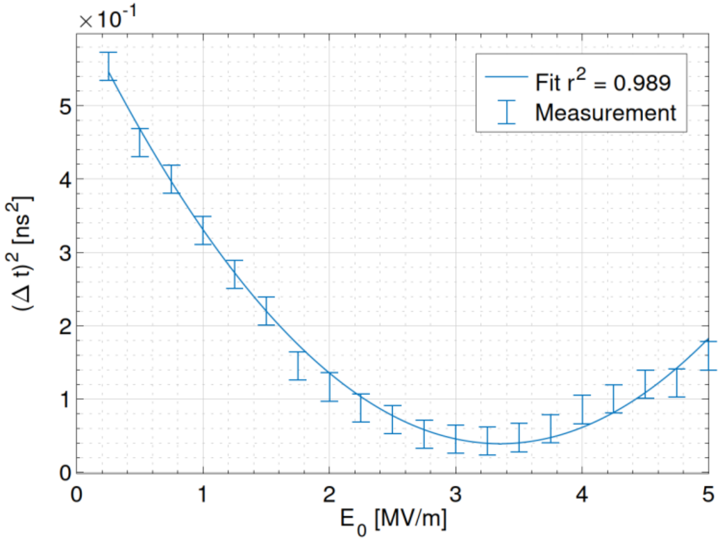

Method Time structure measurement.

Results

Beam Property	From ΔW	From Δt
ε_z [π.ns.keV/u]	1.25(8)	1.18(10)
α_z	-3.54(30)	-4.68(50)
β_z [ns.(keV/u)$^{-1}$]	0.0183(20)	0.0194(30)
γ_z [keV/u.ns^{-1}]	970(40)	1110(50)

"Longitudinal beam properties characterization of very low intensity ion beams at REX/HIE-ISOLDE", N. Bidault, *et al.*, NIM.A, in prep.

Summary

Analysis of REXEBIS performance and produced ion beam quality

- Capability to measure rare contaminants over a wide A/q-range
- Possibility to modulate the macro-time structure of the ion pulse
- Methodology for accessing the axial energy distribution of trapped ions
- Estimation of REXEBIS electron current density for the new electron gun

Post-accelerated ion beam characterization

- Reliability of transverse beam profile measurements in the sub-femto Ampere range
- Methodology for probing the transverse beam properties at very low intensity
- Consolidation of the beam energy measurement technique
- Characterization of the longitudinal phase-space parameters at very low intensity

Selective Bibliography

Physics at ISOLDE

Butler, P. A. et al. (2020). The observation of vibrating pear-shapes in radon nuclei: Addendum. Nature Comm., Vol. 11, 3560 (2020), DOI: 10.1038/s41467-020-17309-y

Leimbach, D. et al. (2020). The electron affinity of astatine. Nature Comm., Vol. 11, 3824 (2020), DOI:10.1038/s41467-020-17599-2

de Groote, R. P. et al. (2020). Measurement and microscopic description of odd-even staggering of charge radii of exotic copper isotopes. Nat. Phy., 16, 620 (2020), DOI: 10.1038/s41567-020-0868-y

Garcia Ruiz, R. F. et al. (2020). Spectroscopy of short-lived radioactive molecules: A sensitive laboratory for new physics. Nature, Vol. 581, 396-400 (2020), DOI: 10.1038/s41586-020-2299-4

Marsh, B. et al. (2018). Characterization of the shape-staggering effect in mercury nuclei. Nature Physics, (2018), DOI:10.1038/s41567-018-0292-8

Rothe, S. et al. (2013). Measurement of the first ionization potential of astatine by laser ionization spectroscopy. Nature Comm., Vol. 4, 1835 (2013)

Gaffney, L. et al. (2013). Studies of pear-shaped nuclei using accelerated radioactive beams. Nature, Vol. 497, 199-204 (2013), DOI: 10.1038/nature12073

Wienholtz, F. et al. (2013). Masses of exotic calcium isotopes pin down nuclear forces. Nature, Vol. 498, 346 (2013), DOI: 10.1038/nature12226

Physics of Electron Beam Ion Sources

Wenander, F. (2010). Charge breeding of radioactive ions with EBIS and EBIT. Journal of Instrumentation, 5(10). DOI: 10.1088/1748-0221/5/10/C10004

Pikin, A., et al. (2016). Analysis of magnetically immersed electron guns with non-adiabatic fields. Review of Scientific Instruments, 87 (11). DOI: 10.1063/1.4966681

Lapierre, A. (2017). Time-dependent potential functions to stretch the time distributions of ion pulses ejected from EBIST. Canadian Journal of Physics, 95(4), 361–369. DOI: 10.1139/cjp-2016-0716

Marrs, R. E. (1999). Self-cooling of highly charged ions during extraction from electron beam ion sources and traps. Nuc. Inst. and Met. B, 149(1–2), 182–194. DOI: 10.1016/S0168-583X(98)00624-7

Fussmann, G. et al. (1999). EBIT: An Electron Beam Source for the Production and Confinement of Highly Ionized Atoms. Adv. Tech., 429–468. DOI: 10.1007/978-94-017-0633-9_19

Currell, F. J. (2003). The Physics of Multiply and Highly Charged Ions. Springer. DOI: 10.1007/978-94-017-00542-4

Shirkov, G. D., & Zschornack, G. (1996). Electron Impact Ion Sources for Charged Heavy Ions. In Electron Impact Ion Sources for Charged Heavy Ions. DOI: 10.1007/978-3-663-09896-6

Fundamenski, W., & Garcia, O. E. (2007). Comparison of Coulomb Collision Rates in the Plasma Physics and Magnetically Confined Fusion Literature. Efda-Jet Report, 07.

Spitzer, L., J. (1952). Equations of Motion for an Ideal Plasma. Astrophysical Journal, 116, 299–316. DOI: 10.1086/145614

Physics of Accelerated Ion Beams

Fraser, M. A. (2012). Beam Dynamics Studies of the ISOLDE Post-accelerator for the High Intensity and Energy Upgrade [University of Manchester]. cds.cern.ch:1423610

Sander, O. R. (2008). Transverse emittance: Its definition, applications, and measurement. AIP Conference Proceedings 212, 127 (May 2008), 127–155. DOI: 10.1063/1.39706

Stockli, M. P. (2006). Measuring and Analyzing the Transverse Emittance of Charged Particle Beams. AIP Conference Proceedings, 868 (December 2006), 25–62. DOI: 10.1063/1.2401393

Wiedemann, H. (2015). Particle Accelerator Physics. In Synchrotron Radiation News (Vol. 7, Issue 4). Springer International Publishing. DOI: 10.1007/978-3-319-18317-6

Wrangler, T.P. (2008) RF Linear Accelerators, 2nd, Completely Revised and Enlarged Edition. Wiley VCH, Physics Textbook. ISBN: 978-3-527-40680-7

Hock, K. M., et al. (2014). Beam tomography research at Daresbury Laboratory. NIMPR A, 753, 38–55. DOI: 10.1016/j.nima.2014.03.050

Thank you for your attention

This work is the result of a collaborative effort involving in particular,

ISOLDE Operation:

Miguel Luis BENITO
Eleftherios FADAKIS
Simon MATAGUEZ
Emiliano PISELLI
Jose Alberto RODRIGUEZ
Erwin Siesling

CERN REXEBIS:

Hannes PAHL
Alexander PIKIN
Fredrik WENANDER

CERN Instrumentation:

William ANDREAZZA
Enrico BRAVIN
Sergey SADOVICH

University of Rome:

Mauro MIGLIORATI

Non-adiabatic immersed electron gun

Design

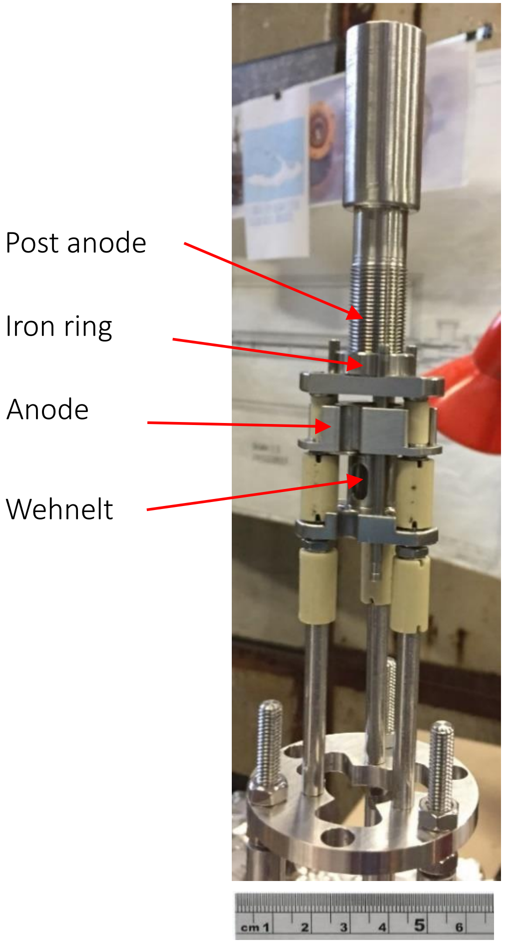

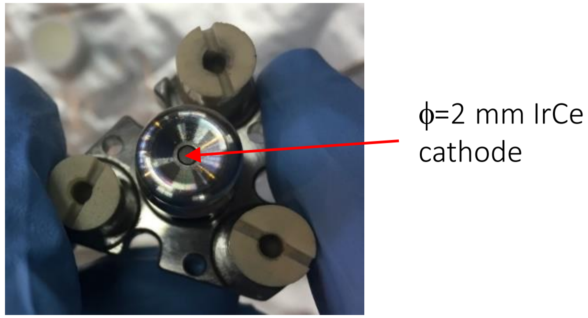

Post anode used to adjustment the phase of cyclotron wrt iron ring for different beam currents

Results

Current and losses

I_e well behaved to 300 mA
<15 uA anode losses
<100 uA losses on drift tube in front of suppressor

EBIS breeding efficiency

19.7% for $^{39}K^{1+}$ to $^{39}K^{10+}$
Almost as high as for old gun

Effective current density

T_{breed}=44 ms for $^{133}Cs^{1+}$ to $^{133}Cs^{31+}$
j_e estimated to ~400 A/cm^2

Problems

1. Excessively high cathode work function (activation not helpful)
2. Electron beam losses rises exponentially when I_e > 300 mA. Believed to be caused by back-scattered or elastically reflected electrons from the collector region.

Non-adiabatic immersed electron gun

- Immersed electron gun positioned in low B-field (few hundred Gauss)
- Reduce cyclotron motion with local magnetic element
- Produce a laminar beam that is thereafter adiabatically compressed by main B-field

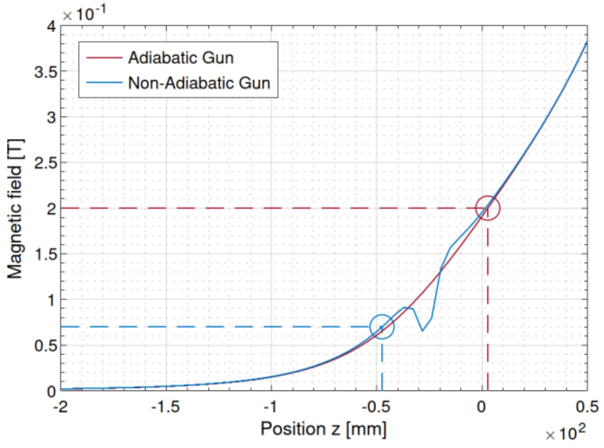

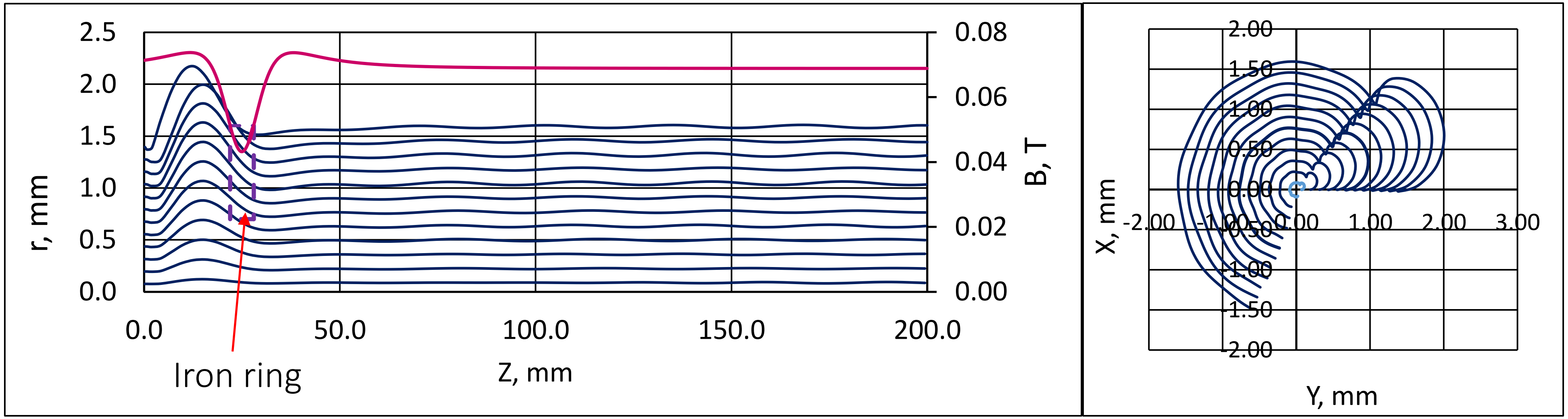

A. Pikin et al., "A method of controlling the cyclotron motion of electron beams with a non-adiabatic magnetic field", accepted PRAB

EBIS plasma: Analytical framework

Kinetic theory applies to classical plasmas that respect the inequations: Landau distance << Interparticle distance << Debye length

Boltzmann Equation

$$\frac{\partial f_i}{\partial t} + \mathbf{v} \cdot \boldsymbol{\nabla}_r f_i + \frac{Q_i}{m_i}(\boldsymbol{E} + \mathbf{v} \times \boldsymbol{B}) \cdot \boldsymbol{\nabla}_v f_i = \left(\frac{\partial f_i}{\partial t}\right)_{\text{coll}}$$

Unique Maxwellian steady state. Collisionless plasma in electromagnetic fields, i.e. Maxwell-Vlassov equation.

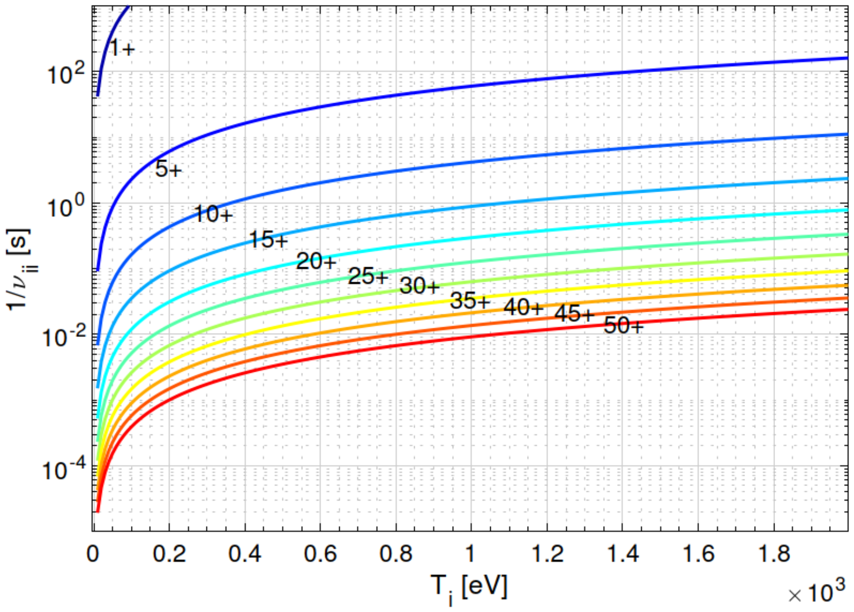

Figure Self collision rate calculated for multi-charged xenon with a density 10^4 mm^{-3}.

Total collision rate

$$\nu_i = \nu_{ie} + \sum_j \nu_{ij}$$

Relaxation to Boltzmann distribution.

Self-collision rate and isotropization

$$\nu_{ii} = \frac{1}{(4\pi\epsilon_0)^2} \frac{4\sqrt{2\pi}}{3} n_i \left(\frac{q_i^2 e^2}{m_i}\right)^2 \left(\frac{m_i}{k_B T_i}\right)^{3/2} \ln \Lambda_{ii}$$

$$T_\perp - T_\parallel \simeq \frac{3T_i}{\nu_{ii}} \frac{\mathrm{d}}{\mathrm{d}t} \ln\left(\frac{B_d}{n_i^{2/3}}\right)$$

Ion Heat Capacity

$$\partial C_V = \frac{\partial E_i}{k_B \partial T_i} = \frac{3}{2} + \frac{q_i}{k_B} \int \frac{\partial \phi(\mathbf{r}) f_i(\mathbf{r})}{\partial T_i} \mathrm{d}\mathbf{r}$$

Degrees of freedom. Trapping effectiveness.

Silicon Detector specifications

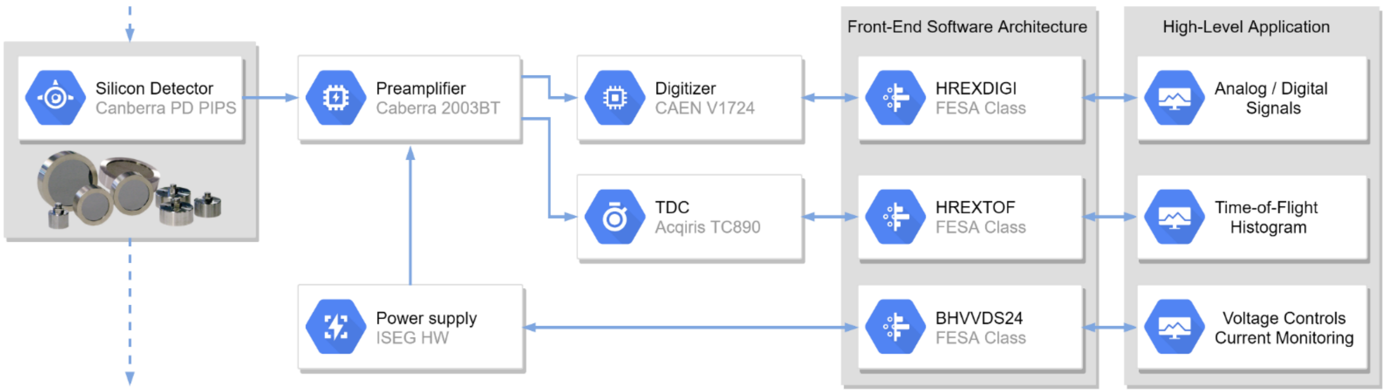

Figures Diagram of the Silicon Detectors DAQ at HIE-ISOLDE.

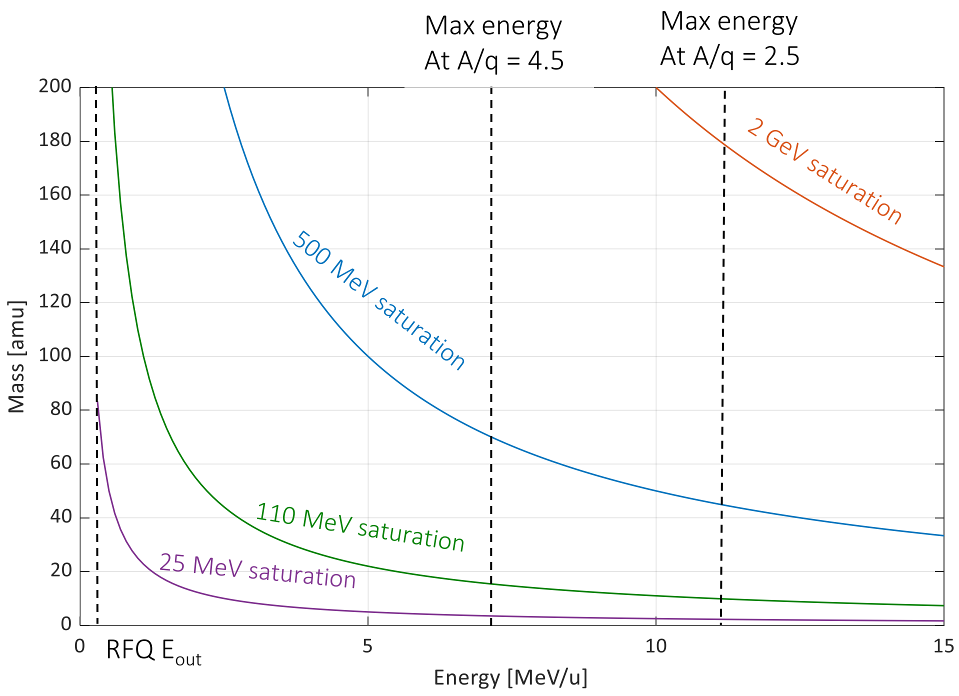

Figure Saturation curves.

Type	Canberra's model	Radius [mm]	Resolution	
			Energy* [keV]	Time [ns]
1	PD50-11-300RM	4.0	11	5
2	TMPD50-16-300RM	4.0	15	0.2
3	PD600-20-300RM	13.8	20	5

Table Basic parameters of 300 µm-thick PD-PIPS detectors used at HIE-ISOLDE (* ^{241}Am, 5.486 MeV alphas).